ANNUAL REVIEWS

Annual Review of Astronomy and Astrophysics

The Character of M Dwarfs

Todd J. Henry[1] and Wei-Chun Jao[2]

[1]RECONS Institute, Chambersburg, Pennsylvania, USA; email: toddhenry28@gmail.com

[2]Department of Physics and Astronomy, Georgia State University, Atlanta, Georgia, USA; email: wjao@gsu.edu

Annu. Rev. Astron. Astrophys. 2024. 62:593–633

First published as a Review in Advance on July 1, 2024

The *Annual Review of Astronomy and Astrophysics* is online at astro.annualreviews.org

https://doi.org/10.1146/annurev-astro-052722-102740

Keywords

exoplanets, M dwarf stars, Solar Neighborhood, stellar activity, stellar populations, stellar properties, stellar rotation

Abstract

M dwarfs dominate the stellar population, accounting for three of every four stars, the nearest of which is Proxima Centauri, the closest destination beyond our Solar System. These cool stars span large ranges in luminosities (one ten-thousandth to 6% $L_\odot$) and temperatures (2,100–3,900 K) and have spectra dominated by absorption bands of titanium oxide (TiO) and, for the latest spectral types, vanadium oxide (VO). They have masses that span 0.075 to 0.61 $M_\odot$, a factor of eight, which is comparable with a spread in masses for dwarf types mid-*B* through *K*. Unlike these more massive stars, in the age of the Universe no M dwarfs have evolved in any significant way. M dwarf systems are multiple roughly one-quarter of the time, with the closest binaries found in orbits that have been circularized via tides for orbital periods of about one week. Unlike any other type of main sequence star, there is a gap in the distribution of M dwarfs near masses of 0.35 $M_\odot$ that pinpoints the separation of partially and fully convective stars, yet both types of M dwarfs are often active, showing both Hα in emission and flares. Many planets are found orbiting M dwarfs, and most of them are terrestrial or neptunian in size, rather than jovian, yet much more work remains to be done to characterize the exoplanet population. Overall, the Solar Neighborhood is dominated by M dwarfs that are likely orbited by many small, as yet unseen, planets—some of which may harbor life very near to that in our Solar System:

- M dwarfs account for three of every four stars.
- M dwarf counts increase all the way to the end of the main sequence.
- M dwarfs are partially radiative at high masses and fully convective at low masses.

Contents

1. INTRODUCTION 594
2. DISCOVERING M DWARFS 595
   2.1. The First M Dwarfs Found 595
   2.2. GJ 1061, A Classic Discovery Tale 596
3. DEFINING M (RED) DWARFS 596
   3.1. The Brightest and Hottest to the Faintest and Coolest 596
   3.2. Spectral Classification: Main Sequence M Dwarfs 599
   3.3. Spectral Classification: M Subdwarfs 602
   3.4. Masses 603
   3.5. Radii 604
4. POPULATION ASPECTS 605
   4.1. Population Based on the 10-Parsec Sample 605
   4.2. Multiplicity 608
   4.3. Orbits 609
   4.4. Red Dwarf Luminosity and Mass Functions 610
   4.5. Metallicities 611
5. STRUCTURE 612
   5.1. Partially Versus Fully Convective M Dwarfs 612
   5.2. The Main Sequence Gap 613
6. ACTIVITY 614
   6.1. Activity Detected Spectroscopically 615
   6.2. Activity Detected Photometrically 618
7. EXOPLANETS 623
8. DISCUSSION 627

1. INTRODUCTION

Hertzsprung–Russell diagram (HRD): a plot showing the distributions of stellar luminosities and effective temperatures

OBAFGKM: letters used to classify spectral types of stars based on features in spectra

M dwarf stars, often called red dwarfs, dominate the population in the Solar Neighborhood, and presumably throughout the entire Milky Way and other galaxies, accounting for three of every four stars (Henry et al. 2006, 2018).[1] Red dwarfs are so intrinsically faint that even though many of them are close by, they are beyond the reach of the naked eye—the brightest red dwarf, Lacaille 9352, has a V magnitude of 7.34, and only four red dwarfs are brighter than $V = 8$. Thus, M dwarfs comprise a stellar swarm that lurks unseen, surreptitiously dominating the Galaxy.

These relatively small, unassuming stars are found in the lower right hand corner of the fundamental map of stellar astronomy, the Hertzsprung–Russell diagram (HRD), along which the main sequence stars stretch through OBAFGKM dwarfs. Compared to our G dwarf Sun, M dwarfs are smaller in diameter by factors of about two to more than ten and have masses comparably smaller. They span a factor of eight in mass—a broader range than the AFGK type stars combined—and although relatively low in mass and small in size, M dwarfs nonetheless provide more mass to our Galaxy than any other single spectral type because of their large numbers. Their photospheres are

[1] Even the quiz show *Jeopardy* in the United States has noted this fact. On August 1, 2023, an answer was given: "THE MOST NUMEROUS TYPE OF STAR IN THE UNIVERSE IS THE RED TYPE OF THIS," to which the correct response is, of course, "What is a (red) dwarf?"

roughly only one-half the temperature of the Sun's, and they are two to four orders of magnitude less luminous. Although the Sun will live roughly 10 billion years, not a single M dwarf has evolved in any meaningful way since its birth over the 13.7 billion years of the Universe's existence. As they continue to form in great numbers in the thin disk of the Milky Way, they also populate the thick disk and halo as effectively pristine, unchanged versions of their original selves. M dwarfs are lonelier than other stars, with only about one in four systems having more than one stellar component (Winters et al. 2019), in contrast to more massive stars that are in multiples 40–100% of the time.

There are, in effect, three types of stars all collected into one spectral type. M dwarfs with masses of 0.4–0.6 $M_\odot$ have partially radiative/partially convective interiors and generally behave in ways similar to their larger K dwarf cousins. Those with masses of 0.3–0.4 $M_\odot$ lie in a transition zone between partially and fully convective stars and have interiors that shift in structure unlike any other type of main sequence star (Jao et al. 2018). The smallest M dwarfs with masses from 0.3 $M_\odot$ down to the stellar/substellar limit at 0.075 $M_\odot$ are fully convective and have molecules in their photospheres, including TiO, VO, and H_2O. Overall, M dwarfs create a wide range of astrophysical characteristics worthy of study and create various types of environments for the many planets that have been found over the past few decades to orbit them.

This presentation is primarily observational in nature, as the many theoretical considerations worthy of attention would expand the article into a very long endeavor. The last treatment focused on very low-mass stars in the *Annual Review of Astronomy and Astrophysics* (ARAA) was the article by Liebert & Probst (1987), which did a superb job of summarizing our knowledge of the smallest stars at the time, with particular highlights including masses for M dwarfs and considerations of just how many very low-mass stars there are in the Milky Way. A comprehensive overview of small stars can be found in the book *New Light on Dark Stars* (Reid & Hawley 2005). Nearly four decades since the last ARAA article, we have learned much about these common denizens of the Solar Neighborhood. In this review, we explore many facets of M dwarfs, from their discovery (Section 2) and the definition of what it means to be an M/red dwarf (Section 3) to various population aspects (Section 4). We probe beyond their photospheres to consider the internal structures of M dwarfs (Section 5) and the consequent activity seen on their surfaces (Section 6), presumably driven by events in their interiors. We then explore the exoplanets currently posited to be orbiting the nearest M dwarfs (Section 7) before summarizing what we know about the most common stellar residents of our Galaxy (Section 8).

2. DISCOVERING M DWARFS

2.1. The First M Dwarfs Found

Pinning down precisely when a star was "discovered to be an M dwarf" is rather difficult because the assignment of M dwarf as a spectral type did not occur until the 20th century, though these small stars were certainly noted much earlier. For example, M dwarfs are not included in the spectral atlas of Morgan et al. (1943), although they presented many M-type giants and subgiants. Likely the first M dwarf cataloged, before the M type had been invented, was Lacaille 9352 (GJ 887, M1.0V; at 3.3 pc, it is the 10th nearest star system). The star was observed by Lacaille in 1752 and measured in 1881 to have a high proper motion of nearly 7 arcsec $year^{-1}$ by Gould (1881). At least two intrinsically fainter stars were identified in the nineteenth century. Lalande 21185 (GJ 411, M1.0V; at 2.5 pc, the 4th nearest) was first cataloged by Lalande in 1801 and is the brightest M dwarf in the northern sky at $V = 7.53$. It was noted to be a high proper motion star by Argelander in 1857 (Lynn 1872) and was listed as type "Ma" by Adams & Kohlschutter (1914), presumably indicative of an M dwarf type. Groombridge 34 (GJ 15 A, M1.0V; at 3.6 pc, the 16th

nearest), was discovered by Groombridge in 1838 and was also noted as type "Ma" by Adams & Kohlschutter (1914).

RECONS: REsearch Consortium On Nearby Stars

Supplemental Material >

The three nearest M dwarfs are Proxima, Barnard's Star, and Wolf 359, each of which has a brief dossier in the **Supplemental Text** of the **Supplemental Material**. All three of these were discovered in the 1910s and remain among the most famous stars known. Proxima is the tertiary in the α Centauri system. Barnard's Star (GJ 699, M3.5V; at 1.8 pc, the 2nd nearest) was discovered by Barnard (1916) and remains the fastest moving star in the sky at 10.4 arcsec year^{-1}. Wolf 359 (GJ 406, M5.5V; at 2.4 pc, the 3rd nearest), was also found because of its large proper motion, 4.8 arcsec year^{-1} (Wolf 1919). Within the next decade, Ross (1926) provided a list of proper motion stars that included three M dwarf gems very near the Sun: Ross 128 (GJ 447, M4.0V; at 3.4 pc, the 11th nearest), Ross 154 (GJ 729, M3.5V; at 3.0 pc, the 7th nearest), and Ross 248 (GJ 905, M4.5V; at 3.2 pc, the 8th nearest), all with proper motions larger than 0.7 arcsec year^{-1}.

Six of the nine stars mentioned here are listed as type "dM" or "sdM" among the 181 stars studied by Joy (1947), whose work focused on spectral types and radial velocities of AFGKM dwarfs. A figure in that paper provides a compelling Russell diagram illustrating M dwarfs on the lower main sequence, and is one of the first references that clearly highlights the nature of these low-luminosity red stars as a group and assigns them the letter M.

2.2. GJ 1061, A Classic Discovery Tale

As time passed, larger and more sophisticated scans of the skies revealed great numbers of M dwarfs. The monumental sky surveys of Giclas et al. (1971) and Luyten (1979) together searched the entire sky to photographic magnitudes of 16.5 for stars with proper motions greater than 0.2 arcsec year^{-1}, most of which were red dwarfs. An example that builds upon that work is the classic discovery tale of GJ 1061 (LHS 1565, M5.0Ve, 3.7 pc), found to be the 20th nearest stellar system 30 years ago (Henry et al. 1994). This star retains that rank among stellar systems today, making it the nearest M dwarf found in three decades, even in the age of the all-sky astrometric surveys of *Hipparcos* and *Gaia* (see Section 4.1). As part of an effort to reveal (primarily) M dwarfs near the Sun that had not yet been identified, the REsearch Consortium On Nearby Stars (RECONS) team targeted GJ 1061 ($V = 13.09$) and three other potential nearby stars based upon photometric parallaxes that placed all four stars nearer than 5 pc. However, optical spectroscopy revealed the others to be distant giants, leaving GJ 1061 as the lone probable nearby star, with a spectrum virtually identical to Proxima's. The final datum confirming the star to be a solar neighbor came from the long-term astrometric work carried out at Siding Spring Observatories (e.g., Ianna & Bessell 1986), which provided a parallax of 273.4 ± 5.2 mas (3.7 pc), thereby proving the star to be less than three times further away than Proxima. This is a classic example of the discovery process for nearby M dwarfs that began with photometric efforts, followed by spectroscopy efforts, and ultimately proven to be nearby via astrometric work that provided the trigonometric parallax.

3. DEFINING M (RED) DWARFS

3.1. The Brightest and Hottest to the Faintest and Coolest

M dwarfs have historically been identified using spectra, for which details are given in Section 3.2. The brightest, hottest M dwarfs are virtually identical to the latest-type K dwarfs, whereas the faintest, coolest red dwarfs are in fact not assigned the letter M. Our understanding of stellar physics has advanced significantly in the past century, and though the spectral type M has been maintained for most red dwarfs, here we extend a bit further to the important astrophysical dividing line between stellar and substellar objects. Hence, throughout this article, when "M dwarf"

is used we in fact mean "red dwarf," which spans spectral types M0.0V through L2.5V. This is warranted because the smallest stars assigned the letter "L" are very similar to the slightly more massive and larger types assigned M9.0V or M9.5V, and we would be remiss if we ignored a few of the faintest, coolest red dwarfs. L dwarfs are separated from M dwarfs by diminishing TiO and VO band strengths while metallic hydride and neutral alkali metal lines appear (Kirkpatrick et al. 1999), yet nearly all objects with types through L2.5 (except for a few young brown dwarfs) are, in fact, stars.

Hydrogen burning limit: the critical mass required to start nuclear fusion

Electron degeneracy pressure: a pressure from fermions that counters gravity seen in both brown and white dwarfs

In contrast to these nuances of letters used for spectral types, absolute magnitudes are clearly defined and often superior when evaluating populations because photometry and parallaxes are now available for far more stars than are high-quality spectra. Furthermore, photometric measurements are usually made using carefully characterized filter sets, whereas spectral types are assigned using different wavelength windows and resolutions by different surveyors. Other advantages of photometric evaluations are the cases of closely separated components in which magnitudes combined with magnitude difference measurements make it possible to characterize components for which individual spectroscopic measurements are difficult, if not impossible, to obtain.

Here, we define red dwarfs by utilizing photometry and parallaxes in concert with spectroscopy to link the characterization to more familiar spectral types. To pin down the bright and faint limits for red dwarfs, we use absolute G magnitudes from *Gaia* Data Release 3 (hereafter GDR3; Gaia Collab. et al. 2023). This choice has been made for several reasons: (*a*) millions of M dwarfs now have measurements at G, far more than the classic V magnitudes measured from the ground, (*b*) *Gaia* provides G band measurements for close multiples down to separations less than an arcsecond in many cases, so individual components can be evaluated, and (*c*) *Gaia BP* and *RP* datasets miss a few percent of stars that have G measurements, so G yields more complete samples.

The three panels of **Figure 1** illustrate observational HRDs for objects within 25 pc. Absolute G magnitudes (M_G) and G–K_s colors are used as proxies for luminosities and temperatures, respectively, where the Two-Micron All Sky Survey (2MASS) K_s magnitudes all have quality code A and objects have been matched to *Gaia* sources using the GDR3–2MASS best neighbors table. Defining red dwarfs requires that two lines be drawn in this HRD, one each at the high- and low-mass/luminosity/temperature ends.

To delineate between K and M dwarfs at the high-mass end, we have collected spectral types from reliable, large surveys of nearby stars, including stars within 40 pc (Gray et al. 2006), the Palomar/Michigan State University survey (Reid et al. 1995, Hawley et al. 1996), and the RECONS group (Henry et al. 1994, 2002, 2006; Riedel et al. 2010, 2014; Jao et al. 2011). Because of differences in methodologies and the typical one spectral class errors in typing near this border, the resulting overlap between late-K and early-M types is evident in **Figure 1*b***. We split the difference here, with roughly equal numbers of interlopers on either side, to set the cutoff for the highest-mass red dwarfs at $M_G = 8.1$.

To separate the smallest stars from the most massive brown dwarfs is rather more subtle than simply selecting a line, as was done between K and M types. Here, we rely on the work of Dieterich et al. (2014), who identified the hydrogen burning limit by using two intersecting characteristics of low-mass stars and brown dwarfs. As mass is removed from a star, its radius shrinks because nuclear fusion rates in its core decrease, whereas as mass is removed from a brown dwarf, its radius expands because electron degeneracy pressure weakens. Thus, there is an inflection point in radius at the border between the lowest-mass stars and highest-mass brown dwarfs, which Dieterich et al. (2014) found to occur at $\sim 0.086\, R/R_\odot$, $\log L/L_\odot \sim -3.9$, and $T_{\rm eff} \sim 2075$ K. These attributes point to the lowest-mass stars having a spectral type of L2.5V. In **Figure 1*c***, we use presumably single objects with spectral types from Best et al. (2020) and plot M dwarfs and L dwarfs, where the latter are a mixture of stars and brown dwarfs. The selected demarcation line at $M_G = 17.8$ is

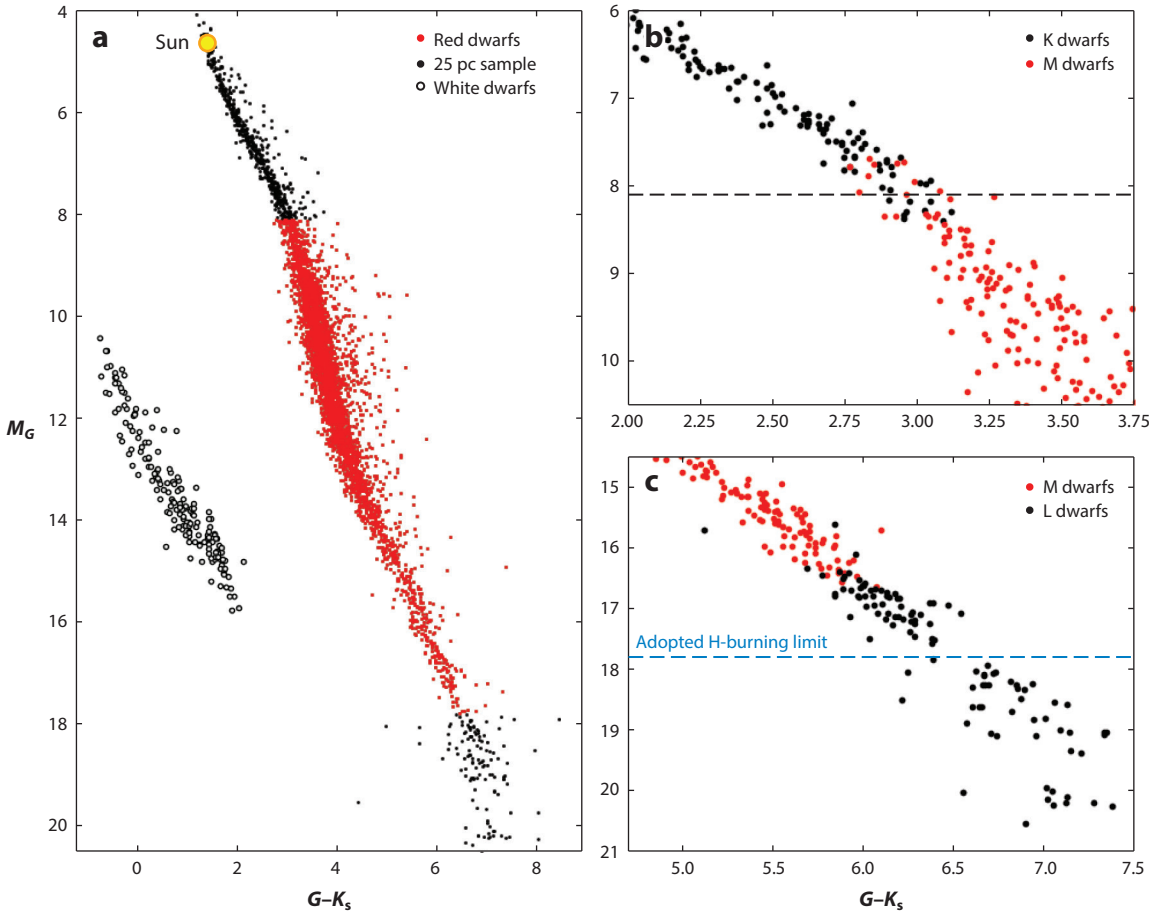

Figure 1

Three different views of the observational Hertzsprung–Russell diagram used to categorize red dwarfs are shown. Panel *a* captures objects within 25 pc from *Gaia* Data Release 3 (Gaia Collab. et al. 2023) having parallax errors less than 0.1%, where red dwarfs are represented by red points. White dwarfs are shown with open circles, and the Sun is marked as a yellow point for context near the top, where the vertical axis has been restricted to highlight red dwarfs. Panel *b* shows the adopted division between stars with spectral types of K (*black*) and M (*red*) at $M_G = 8.1$. Panel *c* shows the adopted hydrogen-burning limit separating the lowest-mass red dwarfs from brown dwarfs at $M_G = 17.8$ for objects with spectral types of M (*red*) and L (*black*). Note that some L dwarfs are stellar red dwarfs. The points in panels *b* and *c* have been carefully vetted to be singles to the extent that is currently possible. Data used to make these three plots are available in the **Supplemental Material**.

Supplemental Material >

drawn where there is an obvious gap in the distribution, and below which the distribution of objects expands, as expected for brown dwarfs having a mix of masses, ages, and atmospheric properties. This division also happens to be the location at which all L2.5V types are above the line, so we select this line to mark the end of the stellar main sequence. There may be a small number of young brown dwarfs above this line, but there should be no stars below it. Age considerations also support the existence of a gap. For a set of objects with ages 0–10 Gyr in the Solar Neighborhood, nearly all of the lowest-mass stars have collapsed to minimal stable radii and M_G values, whereas only a small fraction of the youngest, most massive brown dwarfs will remain "puffy" and have similar M_G while most have already faded to fainter than $M_G = 17.8$.

Table 1 Table of red dwarf characteristics with a comparison to the Sun

Characteristic	Sun G2V	M0.0V	M3.0V	M6.0V	M9.0V	L2.5V
Mass ($M_\odot$)	1.00	0.61	0.28	0.11	0.09	0.075
Luminosity ($L_\odot$)	100%	6%	3%	0.5%	0.02%	0.0001%
Temperature (T_{eff})	5,800	3,900	3,600	3,000	2,400	2,100
M_G	4.66	8.10	10.73	14.25	16.10	17.80
M_V	4.83	8.88	11.99	16.96	19.54	21.61
M_I	4.13	7.03	9.33	12.66	14.56	16.20
M_K	3.27	5.95	6.99	9.44	10.41	11.11
V–I	0.70	1.85	2.66	4.30	4.98	5.41
G–K	1.39	2.15	3.74	4.81	5.69	6.69

Dupuy & Liu (2017) speculated that the hydrogen burning limit may be somewhat cooler than described by Dieterich et al. (2014) owing to possible systematic errors in temperatures derived from model atmospheres. However, using a macro set of more than 300,000 sources within 100 pc, Gaia Collab. et al. (2021) found a dip in the luminosity function at $M_G = 17.6$, which is similar to our line at 17.8. Furthermore, evolutionary models of low-mass objects near the end of the main sequence show rapid temperature and luminosity drops in the first 1–2 Gyr, which is consistent with the empirical gap seen in **Figure 1**. Recent research by Chabrier et al. (2023) focuses on a new equation of state for dense hydrogen–helium mixtures. Although the results do not precisely match the M_G and G–K color values illustrated in the empirical plot in **Figure 1**, the overall trend traces the distribution of points. Their smallest star with mass 0.075 $M_\odot$ effectively settles on the main sequence after 3–4 Gyr, whereas brown dwarfs with masses of 0.074 and 0.073 $M_\odot$ continue to fade, thereby crossing the gap where the line of demarcation has been drawn. Thus, models continue to progress in refining the theoretical definition of the hydrogen burning limit, and the data shown in **Figure 1** provide insightful constraints and a useful guide to the empirical end of the main sequence. We conclude that the HRD gap at $M_G = 17.8$ represents the bridge crossed by brown dwarfs as they cool and grow fainter, slipping down through and eventually off the main sequence of stars.

Table 1 provides general guidelines of red dwarf characteristics, including the high- and low-mass ends at M0.0V and L2.5V, as well as intermediate comparison points at M3.0V, M6.0V, and M9.0V and values for the Sun for context. The values listed in **Table 1** are based upon the RECONS spectral classification system, which is somewhat redder than others at early types (Section 3.2). The result is that for a given type like M3.0V, the values assigned are lower in mass, fainter, cooler, and redder than in other spectral typing systems, although all values are self-consistent within this system. Overall, it is essential to keep in mind that because of the width of the main sequence, these are guidelines and that sets of stars assigned a specific spectral type will vary in the other characteristics listed in **Table 1**.

3.2. Spectral Classification: Main Sequence M Dwarfs

In the late nineteenth century, the "M" spectral designation was first used by Williamina Fleming and a team of women known as the Harvard Computers when they classified spectra for stars in Henry Draper's catalog. The M type was propagated into the Harvard spectral classification system by Annie Jump Cannon (Cannon & Pickering 1918), who added suffixes "a," "b," and "c" to indicate increasing TiO band strengths, a concept that has remained to the present for subtypes of the M class. During the IAU (International Astronomical Union) meeting in 1922, the subtypes of M0 through M10 were introduced using TiO band strengths, and the letter "e" was added to

indicate Balmer line emission, notably for Hα (Adams et al. 1926, Boeshaar 1976). With improving fidelity in spectral classifications, Joy (1947) introduced half-types for M dwarfs, and henceforth, assigning M dwarf types to half units has become the norm, with errors typically quoted to ±0.5 types.

Unfortunately, Joy's classifications lacked spectral standard stars, so spectral types for M dwarfs from low-dispersion photographic plates remained somewhat subjective. The spectral standard stars published by Morgan et al. (1943) could have potentially reduced such problems, but in their atlas, the M type stars only included giants and supergiants for types M0–M4, and no dwarfs. A few M dwarf spectral standards were presented by Johnson & Morgan (1953), but only for M0–M2 types that used TiO band strengths in the blue window (<6500 Å) established by Morgan (1938) and Kuiper (1942) to classify M dwarfs and to indicate effective temperatures.

Boeshaar (1976) extended M dwarf classification spectra to 6800 Å to include additional atomic and molecular lines, adding TiO bands, the VO feature at 5736 Å, and CaOH at 5530 Å, as well as a specific measure of the line ratio of VO at 5736 Å over the TiO band at 5759 Å. An important aspect of her classification system is that it was established by following the effective temperature trend from a set of M giant spectral standards. The Boeshaar system covered types M0V–M6V, stopping before the end of the sequence primarily because the low effective temperatures of late-type M dwarfs shifts the peaks of their spectral energy distributions into the near-IR (a 2,900-K M dwarf's spectrum peaks at 1 μm), and the minimal flux at blue wavelengths made classifying the coolest M dwarfs difficult. The sequence was extended to types M9.0V by Kirkpatrick et al. (1991) using spectra that reached to 9000 Å, taking advantage of the redder limit to reach wavelengths at which the lowest temperature M dwarfs emit significant flux.

In general, the key aspects that separate late K dwarfs from early M dwarfs are that (*a*) the TiO bands are stronger for M dwarfs; (*b*) the CaH and MgH lines are weaker in M dwarfs; (*c*) the Hα line appears in absorption in most K dwarfs, whereas it is often in emission for M dwarfs; and (*d*) VO absorption features are present for dwarfs later than type ∼M5.0V. **Figure 2*b*** illustrates an M dwarf spectral sequence for types M0V through M9V, with key TiO and VO features used for classification highlighted (values for plotting the spectra are given in the **Supplemental Material**). The advent of CCDs (charge-coupled devices) for spectroscopy in the 1990s made it also possible to use the spectral slopes evident in **Figure 2** for classifying M dwarfs, and these slopes, in combination with differences in KI, NaI, and CaII line strengths, can be further used to distinguish M dwarfs from giants (Henry et al. 1997). Various groups have used these features and slopes to assign spectral types for great numbers of M dwarfs. The extensive dataset amassed for the nearest M dwarfs by the RECONS team (e.g., Henry et al. 1994, 2002) enabled the development of an algorithm called `ALLSTAR`, to classify M dwarfs. A full set of RECONS standard stars with spectral types assigned for each 0.5 subtype from M0.0V through M9.0V is given in the **Supplemental Material**. These stars have been selected to be among the brightest representatives of their types: M0.0V–M5.0V stars all have $V < 15$ and M5.5V–M9.0V stars have $V = 13$–19. All but two lie between DEC +30 and −30, so they can be observed from most observatories in both the Northern and Southern Hemispheres. To take advantage of the large set of M dwarf spectra obtained during the Sloan Digital Sky Survey (SDSS), Bochanski et al. (2007) established template spectra of M dwarfs (M0V–L0V) using polynomial relations discussed by Reid et al. (1995) and spectral features such as CaH1, CaH2, CaH3, and TiO5 marked in **Figure 2**. Covey et al. (2007) also used the large SDSS dataset to establish a spectral typing pipeline based on flux-calibrated spectra from Pickles (1998) and derived spectral type versus SDSS color relations. This pipeline is known as "The Hammer" and was later utilized by West et al. (2011) and Lu et al. (2019) to classify a great number of M dwarfs. A noteworthy recent effort on nearby northern M dwarfs that synthesizes earlier results and provides new types is that by

Supplemental Material >

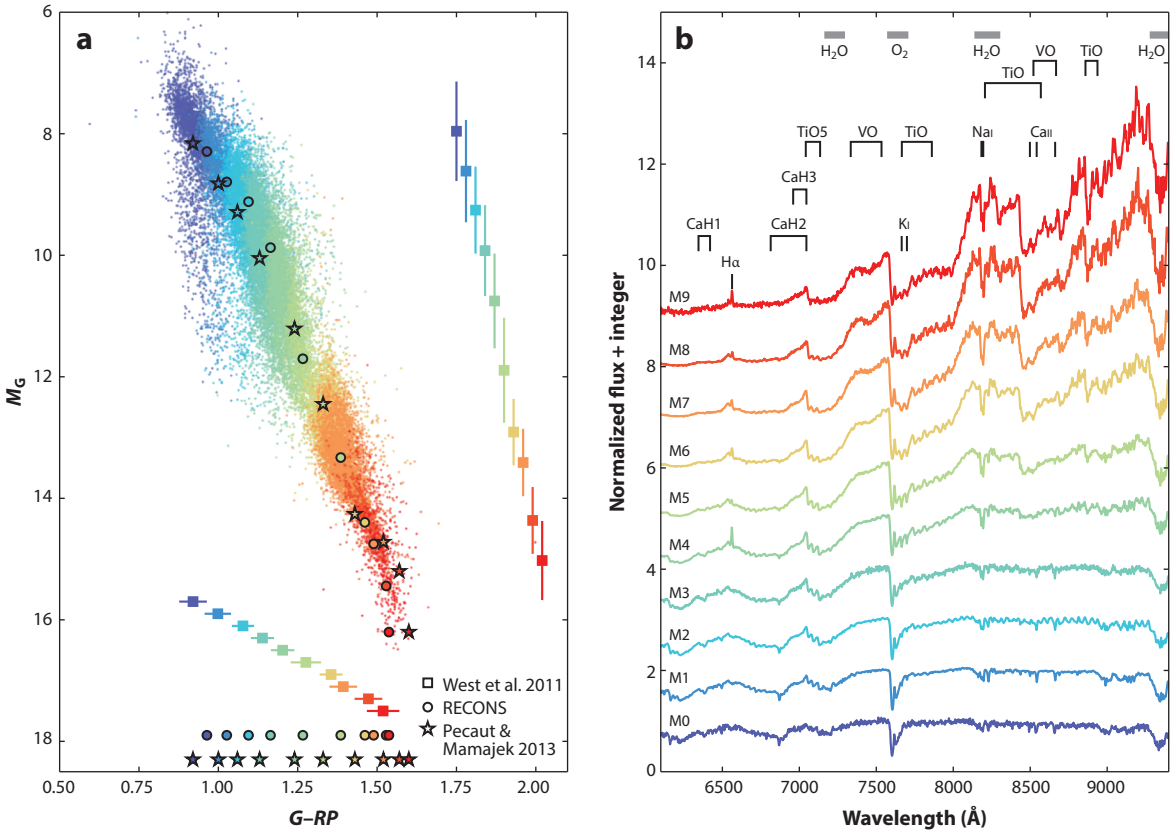

Figure 2

(*a*) M dwarfs classified with types M0V–M9V by West et al. (2011) are shown on an empirical Hertzsprung–Russell diagram, color coded by each of the ten full subtypes; note the subdwarfs below the main sequence. Ten squares along each axis represent mean M_G magnitudes and *G–RP* colors from *Gaia* Data Release 3 (Gaia Collab. et al. 2023) for these types, with error bars showing the standard deviations at each type. Embedded in the main sequence are standard stars for RECONS (*circles*) and values from Pecaut & Mamajek (2013) (*stars*), with projections for each shown along the *G–RP* axis. (*b*) Spectra with resolution of a few angstroms for ten RECONS standard stars. Key spectral features used to establish the sequence are labeled at the top, where prominent telluric absorption regions are noted as gray bars. The color scheme is the same for both plots. The data shown here are available in the **Supplemental Material**. Abbreviation: RECONS, REsearch Consortium On Nearby Stars.

Alonso-Floriano et al. (2015), in preparation for the Calar Alto high-Resolution search for M dwarfs with Exoearths with Near-infrared and optical Echelle Spectrographs (CARMENES) survey.

Supplemental Material >

Figure 2*a* shows M dwarfs from SDSS classified by West et al. (2011), who assigned types using The Hammer, and points are color coded by each full spectral subtype. Ten points along each axis show the mean absolute magnitude and color values for each subtype, with error bars representing the standard deviation ranges. Also shown are circular points representing RECONS spectral types and stars representing types from Pecaut & Mamajek (2013). Overall, the spectral type trends are in agreement among all three systems. The Hammer program yields evenly spaced subtypes, whereas the RECONS and Pecaut sets include specific stars that can be used as standards, so the separations in M_G in particular between specific subtypes vary somewhat, with relatively large gaps on either side of type M4.0V, where the main sequence is the widest. The RECONS set

traces the center of the main sequence and spans a relatively more restricted range in color than the other two sets, whereas the early-type stars in the Pecaut sequence are below the midpoint of the distribution, and the late-type stars are somewhat elevated.

Metallicity, [M/H]: the star's total metal abundance relative to the Sun, where log [M/H] = 0 is defined as solar metallicity

As is evident in **Figure 2*a***, assigned spectral types may differ by two full types for some M dwarfs for a given M_G or *G–RP* value. In the era of *Gaia*, with its high-quality parallaxes and photometry that yield accurate absolute magnitudes, using M_G is arguably better than using spectral types because M dwarfs within hundreds of parsecs can now be precisely placed on the HRD—within 100 pc reddening effects are minimal, and M_G values can be used to select potential M dwarfs even without the spectroscopic determination of types. At least within this horizon, the time-consuming process of securing spectra may not be needed for many research applications, and in fact, M_G values offer higher fidelity in discerning general types of M dwarfs, given the errors in spectral subtypes. Of course, the subtleties of determining youth (Hα), rotation rates ($v \sin i$), and metallicities ([M/H]) can still be explored effectively with spectra, and securing series of spectroscopic measurements remains critical for uncovering companions in radial velocity studies.

3.3. Spectral Classification: M Subdwarfs

Because of their slow evolution, in addition to main sequence M dwarfs there is a set of cool, subluminous M stars that lie below the main sequence that were called "subdwarfs" by Kuiper (1939), a name that is analogous to subgiants for evolved stars. The first three M-type subdwarfs, which have absolute magnitudes 2–3 mag less luminous than main sequence stars of the same color, were reported by Kuiper (1940). The "sd" prefix for these subdwarfs was used by Joy (1947) based on the Mt. Wilson spectral classification system.

The introduction of the "sd" prefix began causing confusion in the late 1940s because "subdwarfs" also began to be used for a class of underluminous blue stars, i.e., types sdO and sdB (Heber 2009). Unlike the old, low-metallicity M subdwarfs, these hot subdwarfs have broad Balmer absorption features or strong HeII lines at 4686 Å, and their locations on the HRD are the product of binary star evolution, with He fusing in their cores. Thus, we are left with the unfortunate situation in which there are two entirely different classes of stars called "subdwarfs"—a hot class that is the result of binary star evolution and a cool set of unevolved single stars that are among the oldest Galactic fossils. The "sd" prefix continues to be used sometimes as part of the spectral type to indicate a cool subdwarf, even expanding to sdM, esdM, or usdM to correlate with ever-lower metallicities (Gizis 1997, Lépine et al. 2007a). Instead, Roman (1955) and Jao et al. (2008) have reasoned that for types later than G0, the spectral notation "VI" should be used for stars that are ∼1–2 mag less luminous than their main sequence counterparts, thereby creating an appropriate luminosity class that separates subdwarfs from main sequence dwarfs.

To identify M subdwarfs spectroscopically, metallic hydride bands such as MgH, CaH, AlH, or FeH can be used because they are sensitive to metallicity. Eggen & Greenstein (1967), Boeshaar (1976), Wing et al. (1976), and Bessell (1982) suggested using metallic hydride band strengths to indicate luminosities and TiO band strengths as temperature indicators. After subdwarfs were identified for a few decades, Gizis (1997) established an M subdwarf classification system based on the metallic hydride bands of CaH1, CaH2, CaH3, and TiO5 (marked in **Figure 2**, although all stars shown are main sequence dwarfs). Lépine et al. (2007a) used a set of more than 400 cool subdwarfs to refine the classification scheme, and a decade later Zhang et al. (2019) proposed using an additional feature, CaOH at 6230–6240 Å, to assist in characterization. Meanwhile, Jao et al. (2008) proposed a spectral classification system that connected atmospheric models to empirical spectra and demonstrated both gravity and metallicity trends on the HRD for subdwarfs.

A few comments related to L subdwarfs are warranted here because a few of these objects may, in fact, be dwarf stars. Lépine et al. (2003) first identified LSR J1610-0040AB to be an L-type subdwarf because it has weak bands of TiO and no detectable VO. This star's classification was later revised to be a peculiar sdM6 (Reiners & Basri 2006), and it was subsequently found to be an astrometric binary (Dahn et al. 2008). A late L-type subdwarf having strong metallic hydride bands and weak TiO bands, 2MASS J0532+8246, was reported around the same time by Burgasser et al. (2003), but it is a brown dwarf. Since then, some stellar L-type subdwarfs with $M_G < 17.8$ have been discovered, e.g., LSR1826+3014 with type sdL0 at 11.0 pc—such objects constitute a small population of the very oldest low-mass stars. Additional details about classifying L subdwarfs are discussed by Kirkpatrick et al. (1999), Burgasser et al. (2003), and Zhang et al. (2018).

Mass–luminosity relations (MLRs): used to relate intrinsic brightnesses of stars to their masses, often using absolute magnitude measurements as proxies for luminosities

3.4. Masses

Mass is the single most fundamental characteristic of a main sequence star because it determines its fuel-burning capabilities and structure. Composition, rotation, and magnetic properties, all of which change via evolution as stars age, are secondary attributes that affect how a star presents itself, but mass remains key to a star's character throughout its life. Given that no M dwarfs have evolved in any meaningful way in the history of the Universe, mass is the primary driver of their fundamental observables, including their temperatures and consequent colors and spectral energy distributions, as well as their luminosities and absolute magnitudes. Although critical to stellar characterization, mass determinations remain one of the most difficult of stellar attributes to pin down, given that the gold standard of model-independent mass measurements remains orbital mapping of binary systems that takes considerable patience and endurance (Serenelli et al. 2021). One technique that has proven to be useful for more massive stars is asteroseismology (Aerts 2021), but M dwarfs do not reveal detectable stellar oscillations useful for such measurements. Nonetheless, we have made progress in determining red dwarf masses, which we now know span a range from 0.61 $M_\odot$ for the hottest types to 0.075 $M_\odot$ for the coolest stars.

Popper's (1980) classic review of stellar masses included only four M dwarfs in two eclipsing systems, but the review by Liebert & Probst (1987) provided a much richer set of 32 stars with masses of 0.07–0.50 $M_\odot$. The first established mass–luminosity relations (MLRs) for M dwarfs in the *VJHK* filters were presented within the relations spanning 0.08–2.0 $M_\odot$ by Henry & McCarthy (1993), where 26 stars with high-quality (at the time) masses less than 0.6 $M_\odot$ were included. Refinements to the *V* relation were made by Henry et al. (1999) using measurements from the fine guidance sensors (FGSs) aboard the *Hubble Space Telescope* and expanded slightly to 33 M dwarfs by Delfosse et al. (2000), who noted that a range of metallicities caused larger scatter in *V* relations than in the near-IR. Very high-accuracy masses with errors of less than 4% for 47 M dwarfs with masses 0.08–0.62 $M_\odot$ enabled by HST/FGS measurements over more than a decade allowed Benedict et al. (2016) to provide more extensive MLRs at *V* and *K*, and that *V* MLR remains the best available today. Dupuy & Liu (2017) extended the mass measurements through the stellar/substellar break with 38 masses of 30–115 M_{Jup}, which were combined with previous efforts and updates to create a list of 62 binaries with mass sums by Mann et al. (2019), from which a new MLR in *K* was derived. Overall, these efforts together result in MLRs at *V* and *K* that can be used to estimate masses of M dwarfs to a few percent on average, although caution must be exercised for individual stars because other stellar attributes will affect the magnitudes observed; e.g., note the width of the HRD in **Figure 1** illustrating that a single absolute magnitude in fact spans a range of color, with variations caused by characteristics other than mass.

The near future holds great promise for an expansive view of M dwarf masses because of the thousands of systems that will soon be available for mass determinations via the precise astrometry

from *Gaia*. Already, high astrometric errors in *Gaia* have been shown by Vrijmoet et al. (2020) to be reliable indicators of multiplicity. Vrijmoet et al. (2022) exploited this result, supplemented by results from long-term astrometry from the RECONS program and the literature, to resolve 211 M dwarf pairs using optical speckle imaging and present an initial set of five new high-quality orbits. The combination of forthcoming *Gaia* astrometric orbits for unresolved M dwarf binaries and high-resolution imaging will yield abundant opportunities for mass determinations and MLRs at *V*, *I* (where in fact, low-mass M dwarfs emit most of their flux), and *K* that are so refined that gradations due to metallicities, and perhaps rotation and magnetic properties, may be teased out. With even better MLRs in hand, the M dwarf masses needed to derive orbiting exoplanet masses will become more reliable, and the characters of those worlds will be better defined.

A reliable relation for low-metallicity M subdwarfs has remained elusive, but shifts in MLRs for these stars are presumably large. As shown by Baraffe et al. (1998), theoretical work implies that M_V for a 0.4-$M_\odot$ dwarf could differ by 1.0 mag between stars with [M/H] = 0 and −0.5, where the lower-metallicity dwarf is brighter. This offset is smaller in the *K* band, so targeted infrared speckle and adaptive optics (AO) work could provide a more straightforward MLR for subdwarfs at near-infrared wavelengths. Alas, similar to the challenges in studying cool subdwarf multiplicity (Section 4.2), very few cool subdwarf binaries have been identified that can be used to establish an empirical MLR (Horch et al. 2015, Jao et al. 2016), so rigorous tests of models at low metallicities remain to be done.

3.5. Radii

M dwarf fundamental parameters also include radii, metallicities, and effective temperatures. Measurements of these parameters have been improved in the past few decades, but unlike measuring masses, derivations of these three parameters are intertwined and require additional assumptions beyond the simplicity of Kepler's Third Law for masses. Accurate radii have become critical because they are needed to determine transiting exoplanet sizes, so there is significant motivation to get the host stars' radii right.

The most common method used to "directly" measure the sizes of red dwarfs, which are no larger than ∼0.6 $R_\odot$, is to observe eclipsing binaries. These doubles may have an M dwarf as a companion to an FGK primary (Gill et al. 2019), two M dwarf components (Torres & Ribas 2002), or an M dwarf with a substellar companion (Irwin et al. 2010). One nearby benchmark M dwarf eclipsing binary is CM Draconis (GJ 630.1 AB, M4.5V+M4.5V, 14.9 pc), a double-lined spectroscopic system with a white dwarf companion at 4.7 arcsec. The near twin components orbit one another in 1.27 days (Morales et al. 2009), have radii of 0.25 and 0.24 $R_\odot$, and are presumably in a tidally locked, synchronized spin–orbit resonance. This is a classic conundrum of eclipsing M dwarfs—to eclipse, the two small stars must be very closely separated, resulting in fast-orbiting, fast rotators that often exhibit frequent flares (Section 6.2), causing challenges for light curve modeling (Martin et al. 2023) and, consequently, radii determinations. Additional complications include having to model spots and limb darkening; i.e., for M dwarfs there is no consensus on appropriate limb darkening corrections that depend on temperature, metallicity, and gravity. Nonetheless, even with these challenges, eclipsing M dwarfs often provide stellar radii reported to accuracies of a few percent (López-Morales 2007, Irwin et al. 2011, Pass & Charbonneau 2023).

The second direct method used to measure the radius of an individual star is long-baseline interferometry. Michelson & Pease (1921) pioneered this technique to measure the radius of Betelgeuse; a valuable description of the method is provided by Lawson (2000). Interferometric baselines at the optical and IR wavelengths at which stars emit most of their flux have been extended to hundreds of meters, and stars as faint as M dwarfs can be reached by facilities such as the CHARA (Center for High Angular Resolution Astronomy) Array and the VLTI (Very Large

Telescope Interferometer). High-resolution efforts with these interferometers have now measured radii accurate to a few percent (Lane et al. 2001, Ségransan et al. 2003, Berger et al. 2006, Demory et al. 2009, Boyajian et al. 2012), with some observations made at near-IR wavelengths at which M dwarf fluxes are increased and limb darkening is less of a concern than at optical wavelengths, although resolution is sacrificed. Combining new measurements and literature values, Boyajian et al. (2012) presented radii of 0.14–0.57 $R_\odot$ for 16 M dwarfs of types M0.0V-M5.0V. Recently, Lachaume et al. (2019) demonstrated an improved algorithm for measuring interference fringes, which could have a significant impact on both radii measurements and their uncertainties for stars smaller than the formal angular resolution limit of the interferometer. Thus, radii measurements may be improved, and uncertainties reduced, in the near future.

However, the M dwarf radii measured are larger than predicted by stellar evolutionary models by 10–15% at a given mass (López-Morales & Ribas 2005, Parsons et al. 2018, Kesseli et al. 2019). This discrepancy has been proposed to be the result of large-scale magnetic fields in these cool stars (López-Morales 2007, Torres et al. 2010), but Feiden & Chaboyer (2014) showed that magnetic stellar models are unable to reproduce the properties of inflated, fully convective M dwarfs. In addition, Kesseli et al. (2019) have shown that neither fast rotation nor duplicity would inflate radii sufficiently to match the models for fully convective M dwarfs. Feiden & Chaboyer (2012) also demonstrated that by revising standard stellar evolutionary models, the radius discrepancy can be reduced to 4% but point out that the uncertainties in empirical radii measurements may be too large to stress-test the models at this level. Another possible cause of the inflated radii in real stars compared to models could be the presence of starspots that could cause stars to appear larger by up to 10%, and cooler by a few hundred degrees Kelvin (Silverstein 2019, Somers et al. 2020), at least for stars with large areal spot coverage. Along these lines, a recent study by Wanderley et al. (2023) shows that models with spots could account for the inflated young M dwarfs in the Hyades, assuming the inflated stars have spots covering 20–40% of their surfaces.

4. POPULATION ASPECTS

4.1. Population Based on the 10-Parsec Sample

Arguably the single most important attribute of M dwarfs is their overwhelming population relative to other stars. Here, we base our understanding of the M dwarf contribution to the stellar population on the census of stars within 10 parsecs, for which the statistics are summarized in **Table 2**. Three out of every four stars—a full 75%—in the Solar Neighborhood are red dwarfs, meaning that they not only constitute the most common type of star but offer by far the greatest number of options for planetary environments and life (see Section 7). In fact, even though

Table 2 Census of stars within 10 parsecs of the Sun

Spectral type	Total	Percentage	Primaries[a]	Companions
White dwarfs	21	5.6%	21	0
A	4	1.1%	3	1
F	7	1.9%	6	1
G	19	5.1%	18	1
K	42	11.2%	27	15
M[b]	280	75.1%	194	86
Total	373	100.0%	269	104

[a]White dwarfs are always assigned to be primaries, given that they originally had more mass than other system components; this includes describing Sirius (type A) and Procyon (type F) as companions.
[b]Includes one *L*-type star.

Lutz–Kelker bias: a statistical effect caused by random parallax errors leading to the underestimation of stars' distances

Malmquist bias: an observational effect that leads to the preferential detection of intrinsically bright objects

individually each star has a relatively thin realm in orbital semimajor axis where temperatures are appropriate for liquid water on planetary surfaces, en masse they include over one-third of all potentially "habitable real estate" (Cantrell et al. 2013). Careful summing of total mass for each stellar spectral type also reveals that, although small, M dwarfs in fact contain more mass than any other type, thereby giving them together outsized gravitational prowess compared to other stars.

Although limited, the 10-pc horizon is the distance to which M dwarfs have been effectively fully discovered and vetted, as both primaries and secondaries, through a combination of more than a century of ground-based parallax work and recent space-based missions. The 10-pc sample has been specifically studied by Kuiper (1942), the RECONS group as detailed by Henry et al. (2006, 2018) and updates at **www.recons.org**, and recently by Reylé et al. (2021). It is important to note that a simple trawl of GDR3 (Gaia Collab. et al. 2023) results will not yield accurate population statistics—of the 269 stellar systems within 10 pc, 22 (8%) do not have astrometric solutions for any of their components in GDR3, including five very bright stars as well as 17 close multiples that contain 36 red dwarf components. So, a GDR3 trawl alone would result in an undercount of red dwarfs by 13%, and the shortfall would be even worse if many of the unresolved red dwarf companions were not uncovered through scrutiny of each higher-mass system.

Ground-based progress through the twentieth century in revealing the population of nearby M dwarfs via their trigonometric parallaxes can be tracked using the series of Yale Parallax Catalogues (YPCs), the fourth edition of which was published by van Altena and colleagues in 1995 (see the electronic version in van Altena et al. 2001). Significant contributors of M dwarf parallaxes in the twentieth century, defined as those providing at least dozens of high-quality measurements, include efforts from the Allegheny Observatory (led by Gatewood), the McCormick Observatory (Ianna), the Sproul Observatory (Heintz), the United States Naval Observatory (Dahn, Monet) the Van Vleck Observatory (Upgren, Weis), and Yale Observatory (van Altena). By the time of the final YPC edition, 122 (63%) of the 194 M dwarf systems within 10 pc had been identified.[2] The final YPC was published before any results were forthcoming from the *Hipparcos* mission, yet additional ground-based efforts after *Hipparcos* contributed many first parallaxes for M dwarfs beyond the spacecraft's faint limit. The largest efforts were those by the RECONS group (Henry, Jao), the Carnegie group (Boss, Weinberger), and the MEarth group (Charbonneau), as well as continuing efforts at the United States Naval Observatory.

After the YPC came the space-based augmentation of the 10-pc sample by *Hipparcos*, the first all-sky astrometry mission that was launched in 1989, which added 18 new M dwarf systems. Yet, the faintest new systems found by *Hipparcos* had $V = 12.2$, leaving many fainter red dwarfs to be discovered. The largest contributor to the population of 10-pc M dwarfs post-*Hipparcos* is the RECONS team, with 36 new systems, whereas all other groups contributed a total of 16 systems. The combination of successful ground-based efforts and the *Hipparcos* sky sweep did not leave (m)any new M dwarf systems to be revealed for the first time by *Gaia*, as it contributed only two new systems to the 10-pc sample, both of which had previous parallaxes placing them just beyond 10 pc. The conclusion is that there remain very few, if any, new stars to be discovered within 10 pc, meaning that the sample is effectively volume-complete—thus, the census numbers presented in **Table 2** are secure. Because of the high precisions of parallaxes and photometry now possible from ground and space, the Lutz–Kelker bias and the Malmquist bias are not relevant for the 10-pc sample, for which the median parallax error is only 0.03 mas, and for which targets have photometric measurements better than a few percent. Predictably, there are no rare O and B stars within 10 pc of the Sun, only modest numbers of solar-type FGK stars, and M dwarfs

[2]A system is considered to be in the 10-pc sample when its parallax is determined to be greater than 100 mas with an error less than 10 mas.

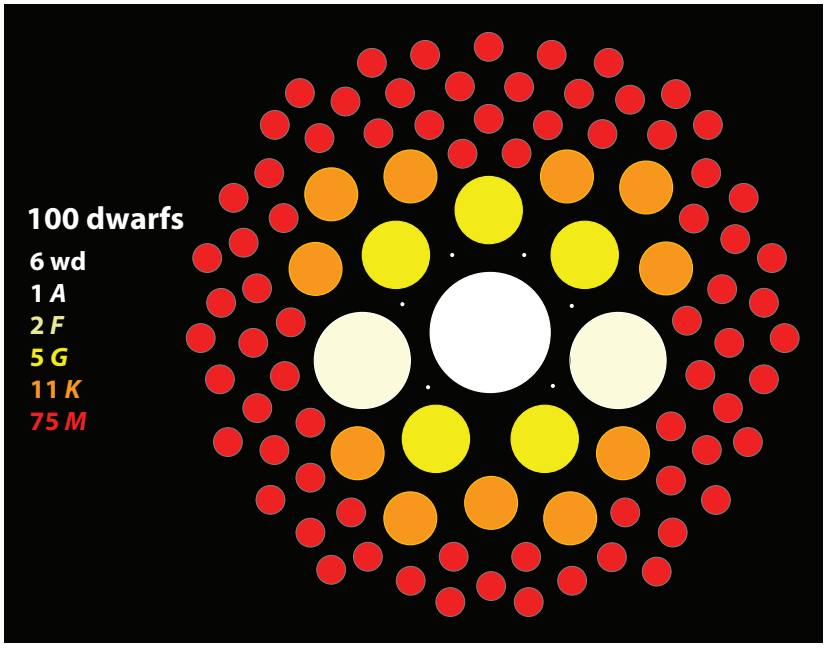

Figure 3

A schematic representation of stellar populations in the Solar Neighborhood, illustrating that M dwarfs account for three of every four stars. The full census numbers for stellar types within 10 pc are given in **Table 2**. There are no O or B stars so close.

dominate the population. **Figure 3** illustrates the population schematically in a convenient form, where 100 dwarfs are used to represent the Solar Neighborhood population, and the counts within those 100 representative stars are shown.

The 10-pc sample offers an initial glance at one of the most difficult of all characteristics to determine for M dwarfs, their ages. Because they are so long-lived, red dwarfs present extreme ages that set them apart from all other types of stars, yet their ages are difficult to discern because the stars remain relatively unchanged since birth. There are two very young and one very old red dwarf systems even within 10 pc of the Sun. The nearest young system is AP Col at 8.4 pc (Riedel et al. 2011), with an age of ∼40 Myr. Found just within the horizon at 9.8 pc, the second young system is AU/AT Mic, a triple set of M dwarfs that is a member of the β Pictoris group with an age of ∼20 Myr. AU Mic is known to be surrounded by a disk and has up to four reported planets (Plavchan et al. 2020, Donati et al. 2023). The binary AT Mic is ∼1.3 deg from the primary on the sky (∼50,000 AU), and the two close components orbit one another in ∼150 years.

At the other age extreme, Kapteyn's Star is the nearest representative of a rare, cool subdwarf close to the Sun, at a distance of only 3.9 pc. With an age of perhaps 10 Gyr or more, it is an ancient, subluminous red dwarf likely from the Galactic halo that is currently moving quickly through the Solar Neighborhood—it has the second largest proper motion (8.7 arcsec year^{-1}) of any star, after only that of Barnard's Star (10.4 arcsec year^{-1}). A likely second subdwarf within 10 pc is CF UMa, also known as Groombridge 1830, although its spectral type is early K rather than M. Given two very young and two very old systems within 10 pc, the rate for each age extreme is about 1% of all systems. Alas, because it is difficult to pin down the ages of M dwarfs, we also do not know the ages of any planets they host. Nonetheless, the population of long-lived red dwarfs provides the

best opportunity for understanding the entire history of the Milky Way because their ages stretch from only a few percent of the age of our Galaxy to fossils that have stood the test of time and have had the full dynamic experience throughout the Milky Way's history.

4.2. Multiplicity

Whether or not any star is solitary or is orbited by other stars, brown dwarfs, planets, or debris provides insight into its formation and evolution. For example, single stars and components in wide binaries are presumably better hosts of planetary systems because disks of material can create planets in stable orbits that are not wrecked by close-in stellar companions. For context, among the members of the 10-pc sample, the 194 M dwarf primaries break down into 141 singles, 41 doubles, 10 triples, 1 quadruple, and 1 quintuple, indicating that 27% of systems are multiple. Of the 53 M dwarf multiples within 10 pc, 49 of the primaries have exclusively red dwarf companions and 4 have brown dwarf companions, implying that brown dwarfs form as companions to red dwarfs less than one-tenth as often as stars.

Many searches for stellar companions to M dwarfs have been carried out, from early IR imaging efforts by Skrutskie et al. (1989; 55 stars) and IR speckle work by Henry (1991; 74 stars) to the HST/NICMOS (Near Infrared Camera and Multi-Object Spectrometer) work of Dieterich et al. (2012; 126 stars), the lucky imaging surveys of Janson et al. (2014; 286 stars) and Cortés-Contreras et al. (2017; 490 stars), and the IR AO study of Ward-Duong et al. (2015; 245 stars). The most comprehensive assessment of M dwarf multiplicity to date is that by Winters et al. (2019), who evaluated all types of M dwarf systems and their companions within 25 pc and provided an overview of 16 previous surveys in their table 1, including all of the surveys just mentioned. Their all-sky examination of 1,120 systems with M dwarf primaries involved new surveys for companions with separations of 2–300 arcsec, augmented with a comprehensive literature search, and yielded a multiplicity rate of 26.8 ± 1.4%, which is identical to the 10-pc fraction. With so many systems surveyed, it was found that there is a broad peak in the separation distribution of the companions at 4–20 AU, i.e., on Solar System scales. Two known caveats reported by the authors are that more than 50 stars appear to have as-yet-unconfirmed close companions that would bump up the multiplicity rate and shift the most common separations to smaller orbit sizes, and that the sample targeted was far from complete, as it was created before *Gaia* results were available.

Future efforts should concentrate on expanded surveys and lower-mass companions, including brown dwarfs and planets of all types. Initial forays into this realm are underway, primarily as radial velocity surveys, e.g., by Delfosse et al. (1999; 127 stars) and Reiners et al. (2018; 324 stars), and speckle imaging studies by Vrijmoet et al. (2022; 333 stars), but the full suite of companions is unlikely to be well understood until a few thousand M dwarfs have been surveyed comprehensively. To this end, the RECONS group is constructing a fully vetted sample of M dwarf systems out to 25 pc, which includes over 3,000 primaries. With such a sample in hand, many groups can combine efforts to discover and explore the myriad companions with masses from 0.6 $M_\odot$ down to terrestrial planets—a factor of a million in mass—with goals of ultimately understanding the star- and planet-formation processes for all types of M dwarfs.

The multiplicity assessments described above include M dwarfs in field samples and provide clues about the distributions of mass ratios and orbit types (Section 4.3). Additional studies that reach further afield address M dwarf multiplicity for younger and older stellar populations. Bergfors et al. (2010) surveyed 124 active, presumably young, M dwarfs and found 44 (35%) to have companions, whereas Janson et al. (2012) expanded on that work and observed 337 similarly active M dwarfs, finding 85 (25%) to be multiple. Because the stars are rather more distant than the Solar Neighborhood sample of Winters et al. (2019) and not all separations were included, these results imply that young M dwarfs may have companions somewhat more often than older field

samples. At the other end of the age spectrum, studying the multiplicity of M-type halo subdwarfs yields clues about the binary-formation history for older populations. The challenges of studying subdwarfs are their intrinsic low luminosities compared to their main sequence counterparts and far lower space densities, forcing surveyors to reach to more distant objects and exacerbating the faint target problem. Since 2000, several small and modest surveys have been conducted for cool subdwarf companions. Initial surveys include those by Gizis & Reid (2000), who used HST/WFPC2 (Wide Field Planetary Camera 2) to observe 11 cool subdwarfs, none of which were resolved; Lépine et al. (2007b), who resolved 1 of 18 M subdwarfs using the AO system at the Lick Observatory; and Riaz et al. (2008), who reported one visual binary using HST/ACS (Advanced Camera for Surveys) among 19 M subdwarfs. Jao et al. (2009) observed a bigger sample of 62 confirmed K and M subdwarfs within 60 pc using optical speckle techniques and determined a multiplicity rate of 26 ± 6%. Ziegler et al. (2015) again increased the size of the sample by selecting 344 subdwarf candidates from a reduced proper motion diagram and resolved 12.5 ± 1.9% of them using the Robo-AO system. Recently, González-Payo et al. (2021) used *Gaia* results to create a list of 214 M and L subdwarfs and found a multiplicity rate of only $1^{+2.0}_{-1.0}$% for projected separations of up to more than 700,000 AU using the GDR3 (Gaia Collab. et al. 2023) catalog; however, this sample will necessarily miss most close companions, so the rate is quite low, as might be expected given that many M dwarf companions are within a few tens of astronomical units (Winters et al. 2019). Although the multiplicity rate remains somewhat unclear for subdwarfs because results vary depending on how the samples are selected and the detection methods, the rate is perhaps lower for M subdwarfs than for field samples, pointing to a likely decreasing multiplicity rate for M dwarfs from young to old stars. Two explanations, both of which may potentially be at play, are that lower-metallicity subdwarfs simply do not form companions as they might in higher-metallicity environments and/or multiples are destroyed over time.

4.3. Orbits

One of the research areas that is advancing quickly at present is the assessment of M dwarf orbits, and a windfall of new orbits is expected in the next few years via future *Gaia* data releases. The first evaluation of M dwarf orbital configurations carried out using the classic eccentricity (e) versus orbital period ($P_{\rm orb}$) plot, which effectively maps orbital shapes and sizes, was presented by Udry et al. (2000), who characterized 48 red dwarf binaries using radial velocity observations. The tidal circularization period appeared to occur around 10 days, and there was a hint of structure in the distribution, implying a lack of circular orbits at longer periods, although the data were sparse. Recent work by Vrijmoet (2023) has expanded the sample to 193 orbits for M dwarf multiples with periods of less than a day to 30 years, corresponding to orbital semimajor axes <10 AU. Vrijmoet finds that the orbital circularization period for M dwarfs is around 7 days, which is much shorter than the ∼12-day period for solar-type stars. It also appears that there are very few systems with $P_{\rm orb}$ = 5–30 years in circular orbits. The few systems with $e < 0.1$ all have at least one component of very low mass, suggesting that their early dynamical evolution is dominated by migration through circumstellar disks, whereas more massive systems do not end up in nearly circular orbits.

As discussed in the work of Winters et al. (2019), which targeted 310 M dwarf pairs, many of which were too wide to have orbits, and additional closer systems studied by Vrijmoet (2023), the mass ratios of M dwarfs in multiple systems point to equal mass systems being the most common; i.e., mass ratios $q \sim 1$. This is particularly true for the close systems. The distribution for $q = 0.5$–0.9 is relatively flat for both samples, and then for mass-discordant systems with $q < 0.5$ there is a tail off to lower masses and virtually no systems with $q < 0.1$. A caveat noted by both sets of authors is, however, that the high-mass ratio systems are the most difficult to detect in both imaging and

radial velocity surveys, although in the latter case the efforts by Baroch et al. (2018) and Winters et al. (2020) have recently added important spectroscopic binaries via sensitive searches. Thus, a key area of future work is to target a volume-complete sample of M dwarfs to prevent biases and to reach as far down in mass for companions as is feasible to reveal the true natures of the mass ratios between these stars and their companions.

4.4. Red Dwarf Luminosity and Mass Functions

Here, we evaluate the red dwarf members of the population relative to one another in the forms of their luminosity function (LF) and mass function (MF), both of which illustrate the extreme differences between the largest and smallest types of these small stars. The LF at optical wavelengths has been known to turn over for nearly a century (Luyten 1938, 1968; Reid et al. 1995; Gaia Collab. et al. 2021), although shifts occur in the precise peak locations owing to the choice of filter bandpass, the parallax sets available at various times, and treatments of unresolved multiples. As discussed above, mass is the most critical aspect of a star, so the MF is therefore the more important snapshot of the diversity of the M dwarf population. Work on the MF for red dwarfs has led to conflicting interpretations: Scalo (1986), Reid (1987), and Bochanski et al. (2010) concluded that the MF turned over, typically reaching a peak near 0.2–0.3 $M_\odot$, whereas Dantona & Mazzitelli (1986), Henry (1991), and Winters et al. (2019) contended that the MF increases down to at least 0.1 $M_\odot$. Particularly revealing is that the latter study reached out to 25 pc to include more than 1,000 M dwarfs before *Gaia* results were available, and even though the sample was known to be incomplete, the MF was clearly rising to the lowest masses.

As discussed in Section 4.1, the modern 10-pc sample is ideal for deriving the most accurate stellar population statistics because the 269 systems of all spectral types within 10 pc have been completely searched and vetted for at least companion stars in long-term astrometry, radial velocity, AO, and speckle imaging surveys. However, the 280 M dwarfs within 10 pc constitute a relatively small population. In order to bolster the statistics for LF and MF, here we reach a bit further and focus on red dwarfs with parallaxes of at least 60 mas,[3] creating a list of nearly 1,000 M dwarf systems (by Madison LeBlanc). *Gaia* provides key additions to this more distant horizon of 16.7 pc, where $G = 18.9$ for stars at the end of the main sequence at $M_G = 17.8$, resulting in a sample that is comfortably brighter than *Gaia*'s detection limits. The sample has been constructed using GDR3 (Gaia Collab. et al. 2023) and supplemented with additional systems with parallaxes from other sources, but as presented here includes only systems with red dwarf primaries. As pointed out by Henry & McCarthy (1990) and reaffirmed by Winters et al. (2019), deblending multiples is critical when determining accurate LF and MF distributions, so we provide the results for a deblended 16.7-pc sample to the extent that it can be done. This is largely possible for systems in which the M dwarf is a primary, but systems with more massive primaries often have secondaries that have never been imaged, e.g., single-lined spectroscopic binaries, so their character remains uncertain. There are anticipated to be fewer than 100 of these M dwarf companions to higher-mass stars in the sample, but more work is needed to place them into the histograms in **Figure 4**, so they are omitted for now. Where G is not available for individual stars, V or I magnitudes were used because deconvolutions are available in these filters (Henry et al. 1999, Vrijmoet et al. 2022), and conversions have been made between filters using more than 500 presumed single stars with individual V, G, and I photometry. Even so, of the 941 M dwarf systems within 16.7 pc, 71 have companions that have yet to be imaged at any wavelength, so these are in a set of blended systems. This volume-limited sample is not yet perfect, but is anticipated

[3]As with the 10-pc sample, Lutz–Kelker and Malmquist concerns are not relevant because of the high accuracies for parallax and photometric measurements for stars within 16.7 pc.

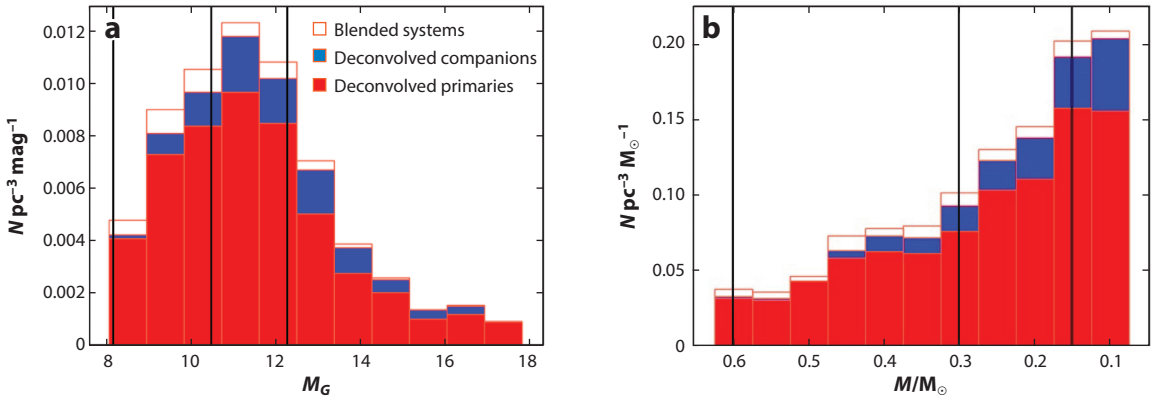

Figure 4

Distributions in stellar characteristics for the red dwarf population within 16.7 pc are shown. (*a*) LF (bins 0.88 mag in width) in the *Gaia G* band. (*b*) Mass function (bins 0.05 $M_\odot$ in width) after converting each star in the LF to a corresponding mass. The 870 deconvolved primaries (*red*), 170 deconvolved companions (*blue*), and 71 blended systems (*white*) are shown in both plots. Once split, the blended components will sprinkle to the right of their locations, which is a focus of future work. Vertical black lines are drawn at factors of two in mass (and corresponding M_G values) at 0.60, 0.30, and 0.15 $M_\odot$, with the end of the least massive bin at 0.075 $M_\odot$. Values used in these plots are available in the **Supplemental Material** in **Supplemental Table 2**. Figure provided by Madison LeBlanc. Abbreviation: LF, luminosity function.

to be missing only a few percent of red dwarfs, and we deem this deeper pool to be representative of the M dwarf population for the LF and MF.

The LF for the lowest-mass stars is illustrated in **Figure 4*a***, with primaries shown in red, companions in blue, and blended systems in white. Future work will allow blended systems to be split into two or more components that will be sprinkled to fainter M_G in the histogram. As has long been known, the LF turns over at optical wavelengths, with at peak in this filter being near $M_G = 11$. There is a steady decline toward more luminous, massive stars (as expected) and a gradual tail stretching to the lowest-mass stars.

Supplemental Material >

The more insightful MF is shown in **Figure 4*b***, again with primaries in red, secondaries in blue, and blended systems in white. As always, it is prudent to keep in mind that no M dwarfs have evolved significantly in the age of the Universe, so this MF also represents the IMF (initial mass function). To determine the MF, a mass for each star in the LF is derived utilizing the mass–luminosity relation of Benedict et al. (2016) in the *V* band, with appropriate conversions from M_G and M_I to M_V as needed. The result is a clear rise in the MF all the way to the end of the stellar main sequence, with the numbers doubling from 0.6 $M_\odot$ to 0.3 $M_\odot$, to 0.1 $M_\odot$. The next critical work related to the LF and MF is to evaluate what happens as the stellar/substellar border is crossed. However, this will be difficult because just below the break are brown dwarfs that have fading luminosities over time, and there is no single mass–luminosity relation that can be used to convert easily measured absolute magnitudes into masses.

4.5. Metallicities

Metallicity is a key factor that affects the character of M dwarfs. Certainly, cool M subdwarfs have emergent spectra that are noticeably different than their main sequence counterparts, affecting their colors, luminosities, and positions on the HRD. Metallicity measurements enable the exploration of (*a*) the range metallicities among nearby M dwarfs (Hejazi et al. 2022); (*b*) the impact of metallicities on fundamental stellar parameters, i.e., radius and mass (Boyajian et al. 2012,

Mann et al. 2019); (*c*) the formation of exoplanets in different metallicity environments (Fischer & Valenti 2005, Newton et al. 2019); and (*d*) the correlations of metallicities with Galactic kinematics (Medan & Lépine 2023).

The measurement of M dwarf metallicity requires a grid of model atmospheres to which acquired spectra can be compared. Surprisingly, the first M dwarf for which a metallicity was measured was Kapteyn's Star (Mould 1976b), which is now known to be a metal-poor star with relatively weak TiO bands. The Fe and Ti lines between 8400 and 8800 Å and his own grid of spectra (Mould 1976a) were used to determine a metallicity of [M/H] = −0.5; modern methods have resulted in a revised value that is much more metal-poor, [M/H] = −1.5 (Woolf & Wallerstein 2004). Since Mould's initial work, establishing reliable spectroscopic models and the techniques used to measure metallicities for M dwarfs have evolved together.

The leading atmospheric models for M dwarfs are `PHOENIX/BT-Settl`, `ATLAS`, and `MARCS` (Hauschildt et al. 1999, Castelli & Kurucz 2003, Gustafsson et al. 2008, Allard 2014), which are all used to generate synthetic spectra. Stellar parameters are then derived by comparing these synthetic spectra to observations via general χ^2 fitting (Gizis 1997) or by using software like `MOOG` (Sneden 1973) or `Spectroscopy Made Easy` (Valenti & Piskunov 1996). Generally, M dwarf abundances can be measured using high- or low-resolution spectra at optical or near-IR wavelengths (Woolf & Wallerstein 2005, Rojas-Ayala et al. 2012). Recently, more advanced algorithms like machine learning have been utilized, and reviews of different techniques of measuring M dwarf metallicities are presented by Lindgren & Heiter (2017) and Passegger et al. (2022). Due to the complexities of opacities for molecules like TiO and H_2O found in M dwarf atmospheres, metallicities of the primaries in binaries with M dwarf secondaries are sometimes used because the FGK dwarfs often have well-calibrated atmospheric models (Bonfils et al. 2005, Montes et al. 2018, Souto et al. 2020) and reliable metallicity determinations. After these benchmark M dwarf metallicities are measured, metallicities for much larger samples can be derived using comparative spectral indices or lines (Woolf et al. 2009, Mann et al. 2014, Marfil et al. 2021). Overall, the results indicate that M dwarfs have metallicities not terribly different from the Sun's, with a trend toward the population having slightly fewer metals.

5. STRUCTURE

5.1. Partially Versus Fully Convective M Dwarfs

In the early 1950s, astronomers encountered difficulties when attempting to apply a stellar interior model similar to that of the Sun, featuring a radiative core surrounded by a convective envelope, to M dwarfs. For example, Stromgren (1952) pointed out the need to investigate the extent of the convection zone in stars like Kruger 60A (GJ 860 A, M3.0V, 4.0 pc) that have masses much smaller than the Sun's, because such stars have significantly lower temperatures and it was necessary to reevaluate their equation of state, energy production methods, and opacities. Osterbrock (1953) successfully employed the solar interior model for some smaller stars, incorporating an extended outer convective envelope for α Cen B (GJ 559 B, K1V, 1.3 pc) and the eclipsing binary Castor C (GJ 278 C, M0.0V, 15.1 pc), but the model was still unsuccessful in matching the observed luminosity, mass, and radius for the lower-mass star Kruger 60A. Thus, disparities between observations and theory persisted and continued to challenge our understanding of interior structure, stellar opacity, energy generation and propagation, and equation of state for low-mass M dwarfs. Continued advances in theoretical work (Limber 1958, Dorman et al. 1989, Baraffe et al. 1997) resulted in models with fully convective interiors for M dwarfs with a boundary transition near spectral type M3V, where the interior structure transitions from partially convective to fully convective. Yet, locating the transition zone observationally remained elusive.

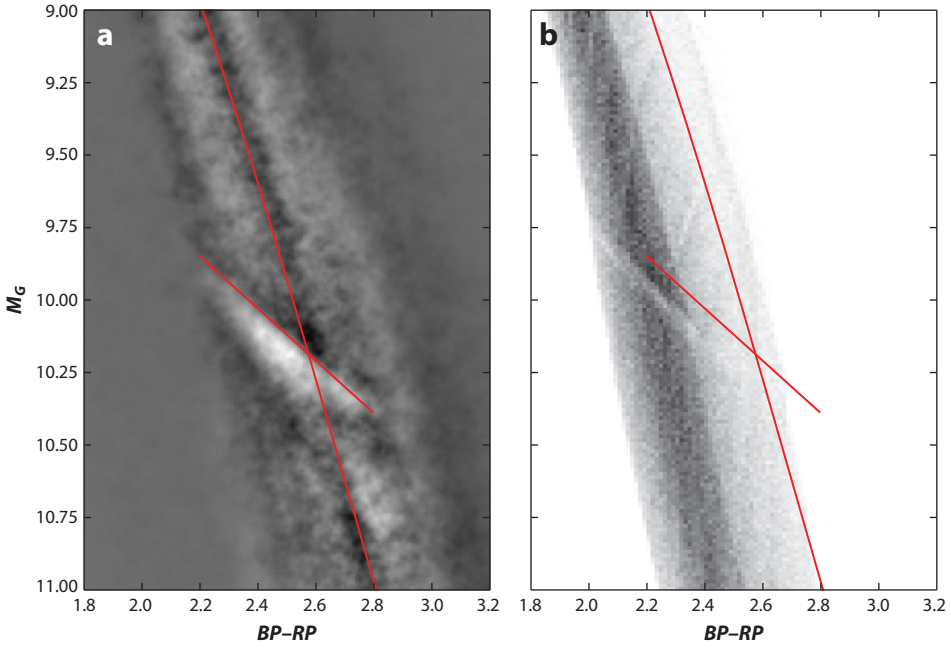

Figure 5

(*a*) An enhanced portion of the main sequence on the observational Hertzsprung–Russell diagram for M dwarfs is shown. The nearly vertical red line represents the middle of the main sequence. The gap is shown as a low-density region in white and the short red line represents the top edge of the gap given by Jao et al. (2023). A second low-density region identified by Jao & Feiden (2021) can be seen on the lower right side of the gap. (*b*) A simulated main sequence for M dwarfs near the gap is illustrated. The two red lines are the same as those in panel *a*, and the theoretical location of the gap is seen as a narrow white strip to the blue side of the red line. Panel *a* adapted from Jao & Feiden (2021). Panel *b* adapted from Feiden et al. (2021).

5.2. The Main Sequence Gap

The extensive set of stars with high-precision photometry and parallaxes in *Gaia* Data Release 2 (Gaia Collab. et al. 2018) enabled a detailed study of the HRD around the location of the transition zone. By mining the rich GDR2 dataset, Jao et al. (2018) discovered a thin gap in the stellar distribution in the lower main sequence, reproduced in **Figure 5*a***, and proposed that the gap marks the transition boundary between partially and fully convective stars. Soon thereafter, MacDonald & Gizis (2018), Baraffe & Chabrier (2018), and Feiden et al. (2021) provided an explanation for the feature—the mixing process of ^{3}He, which is produced in the proton–proton I chain during the merger of the upper envelope and core convection zone. Their models independently confirm earlier work by van Saders & Pinsonneault (2012), who outlined this convective core instability. Models now indicate that low-mass stars in a narrow mass range experience a convective layer instability, consequently producing emergent fluxes that fluctuate over time. The gap spreads across the main sequence because of variations in metallicity that affect luminosities and colors. M dwarfs above the gap do not experience this mixing process and host solar-like interiors, with a radiative core and convective envelope. Stars in the gap go through multiple phases that together are called a "convective kissing instability," as a thin radiative layer forms and disappears until the ^{3}He abundance stabilizes (van Saders & Pinsonneault 2012, Baraffe & Chabrier 2018). M dwarfs below this gap are fully convective throughout their lives. Thus, a few decades after predicting that there must

be a transition region, the discovery of the gap on the HRD pinpointed the boundary between partially radiative and fully convective M dwarfs near 0.31–0.38 $M_\odot$ for the first time.

The α effect: twisting of magnetic field lines by rotation; transforms a toroidal field to a poloidal field

The Ω effect: winding of poloidal magnetic field due to differential rotation, transforming a poloidal field to a toroidal field

M dwarfs above the gap have solar-like interiors with a tachocline separating the inner radiative and outer convective layers, resulting in a similar $\alpha\Omega$ dynamo—a combination of the α effect and the Ω effect—like the Sun's (Charbonneau 2014). Fully convective M dwarfs below the gap have a different α^2 dynamo (Chabrier & Küker 2006); magnetic dynamos for M dwarfs are discussed further in Section 6.2.2. Stars in the gap have tachoclines that form and disappear until the ^{3}He abundance stabilizes, resulting in a potential "switching" magnetic dynamo that changes between $\alpha\Omega$ and α^2 versions, with timescales depending on the stars' evolutionary paths and rotation rates. This implies that stars near the boundary have unstable structures and likely experience abrupt changes in their large-scale magnetic topologies (Donati et al. 2008, Reiners & Basri 2009) and may be expected to exhibit observable effects such as photometric variability and/or fluctuating Hα emission strengths. To date, no observable switching magnetic dynamo effects have been confirmed; e.g., Jao et al. (2023) showed that there is no Hα activity anomaly for stars in the gap, suggesting that the internal instabilities in these M dwarfs have minimal impact on Hα emission.

Previous prominent features on the HRD—the Hertzsprung gap, the Henyey track, and the Hayashi track—are all related to stellar evolution phases exhibited by young stars settling onto the main sequence or by mature stars evolving off of the main sequence. In contrast, the partially/fully convective gap is part of the life of main sequence stars and allows for simultaneous tests of M dwarf atmospheric physics and interior physics in theoretical models. **Figure 5*b*** illustrates results from Feiden et al. (2021), who created a simulated set of 1.1 million dwarfs with masses between 0.1 and 0.8 $M_\odot$ using the Dartmouth stellar evolution model (Feiden 2016) and `MARCS` atmospheric model (Gustafsson et al. 2008), and plotted them on an HRD using *Gaia* magnitudes. Although the main sequence and gap are shifted blueward, the slope of the modeled gap matches that observed. Boudreaux & Chaboyer (2023) attempted to align the observed and modeled gap positions by comparing two opacity models, `OPAL` and `OPLIB`. They found that although the `OPLIB` model exhibited a better fit to the predicted location of the gap, it was still not a perfect match, and they concluded that the improvement might be too subtle to be observable in empirical data. To study the long-term pulsations of the M dwarfs, Mansfield & Kroupa (2021) applied `MESA` stellar evolutionary models utilizing fine mass and time steps and various metallicities, and included a discontinuity in the MLR in the transition zone. Although a direct comparison between the positions of the modeled and observed gaps was not done, this study revealed distinct stellar evolutionary loops in luminosities and effective temperatures on the HRD. Collectively, these studies underscore ongoing challenges faced by theoretical models in accurately reproducing the gap in the HRD. Further research is necessary to refine these models, with a particularly useful near-term focus on determining the masses of stars just above, in, and just below the gap. Regardless of the status of theoretical work, what has become clear is that by combining the location of the partially/fully convective gap with the stellar mass function for red dwarfs (Section 4.4), roughly 50% of all stars are fully convective.

6. ACTIVITY

Every M dwarf is active at some level; detectability just depends upon what characteristic is being measured, the sensitivity level reached, and the cadence of the observations. One of the earliest documented instances of M dwarf activity is that of Luyten (1926), who reported a decrease in the strength of the Hγ line of AT Mic (GJ 799 AB, M4.0e+M4.0e, at 9.7 pc), and estimated the photometric variability for the pair of pre–main sequence stars taken in 1895 and 1903 to be less than 0.5 mag. Over a decade later, van Maanen (1940) reported a sudden flaring event of 1.6 mag in

the nearby red dwarf WX UMa (GJ 412 B, M5.5Ve, 4.9 pc) while measuring its parallax. In 1948, Edwin Carpenter detected an outburst from the M dwarf secondary in the L 726-8 system (UV Ceti, GJ 65 B, M5.0V, 2.7 pc), with a brightening by 1.85 mag based on consecutive photographic plate images (Luyten 1949). In the same year, Joy & Humason (1949) also observed L 726-8 B and noted strong emission in the Balmer and CaII (H and K) lines.

In 1958, the second edition of the *General Catalog of Variable Stars* (Kukarkin & Parenago 1958) introduced a distinctive class of "eruptive stars" as "UV Ceti Variables." These stars were characterized by spectral types in the range of M3V–M6V and exhibited short-duration brightness increases of up to 6 mag at optical wavelengths, with outbursts lasting for tens of minutes. These events have come to be known as flares. Since these initial discoveries, the population of flaring or "active" M dwarfs has grown considerably and research has kept apace, encompassing studies on the formation mechanisms and modeling of the outbursts (Kippenhahn & Schlüter 1957, Allred et al. 2015) as well as activity statistics in large samples derived from various surveys, such as SDSS (West et al. 2011), CARMENES (Alonso-Floriano et al. 2015), *Kepler* (Davenport 2016), GALEX (*Galaxy Evolution Explorer*; Miles & Shkolnik 2017), TESS (*Transiting Exoplanet Survey Satellite*; Günther et al. 2020) and LAMOST (Large Sky Area Multi-Object Fibre Spectroscopic Telescope; Zhang et al. 2021).

M dwarfs are usually identified as active flare stars by monitoring brightness changes photometrically, or spectroscopically by examining the Hα feature. However, the Hα equivalent widths used to distinguish active versus inactive M dwarfs vary among different studies. For example, West et al. (2008), Newton et al. (2017), and Jeffers et al. (2018) set different thresholds for active stars at equivalent width values of 1 Å, −1 Å, and −0.5 Å, respectively, owing at least in part to different spectral resolutions used for the spectroscopic observations. Recently, Kiman et al. (2021) employed a color-dependent (*G–RP*) polynomial relation to define active and inactive M dwarfs, instead of adopting a fixed threshold. These different thresholds and techniques pose challenges when attempting to combine these datasets and are confounded by the fact that the Hα feature itself is likely to vary in time, especially for active stars. In addition, stars that are found to be inactive via these observations may, in fact, be active at other wavelengths, notably in the UV (Youngblood et al. 2017). This implies that different wavelengths and features probe different energy sources and levels within stellar atmospheres.

Our understanding of stellar activity stems primarily from our knowledge of solar dynamo processes, with stellar flares generally attributed to the rapid release of energy through magnetic field reconnections. Reviews on this topic can be found in articles by Benz & Güdel (2010) and Basri (2021), and this magnetic activity can be detected spectroscopically or photometrically across a wide range of wavelengths, from X-rays to radio. In the following discussion, we outline M dwarf activity observed via both spectroscopic and photometric methods and examine how they may be connected.

6.1. Activity Detected Spectroscopically

Pioneering work by Joy (1947) not only initiated the spectral classification process for M dwarfs (Section 3.2) but also reported magnetic activity measured by the appearance of Hα in emission, designating stars with this feature as dMe. This line at 6562.8 Å is commonly used to diagnose magnetic activity in stellar chromospheres and is particularly useful for M dwarfs, but the interpretation of its line strength is rather more difficult than for some other spectral lines. First, the formation of the Hα line could be from collisional excitation or recombination and cascade after photoionization (Linsky et al. 1982). Second, Cram & Mullan (1979) and Stauffer & Hartmann (1986) showed that as chromospheric heating increases, the Hα line absorption first grows deeper,

S-index: a measurement of the emission line cores of CaII H and K lines normalized by two adjacent continuum bands

then fills to become an emission feature. Hence, the maximum absorption depth may not indicate the most quiescent state of a star, and the depth measured is in fact mass-dependent (Newton et al. 2017), so a measured Hα absorption equivalent width may provide ambiguous information on stellar magnetic activity.

When evaluating M dwarf activity levels, samples are often separated into active or inactive groups by their Hα equivalent widths. The four panels of **Figure 6*a*** illustrate the distributions of inactive and active early/mid-type M dwarfs using Hα measurements. Note that the coolest M dwarfs, which reach to $M_G = 17.8$, are not represented here. The inactive stars have a distribution centered on the main sequence, whereas active stars are clearly elevated, as reported by Jao et al. (2023), who also revealed an Hα activity deficiency region marked in the rightmost subpanel of **Figure 6*a*** (discussed further in Section 6.2.2). Both active and inactive stars are found in every spectral subclass of M dwarfs, with the percentages of active M dwarfs generally increasing from hotter to cooler M dwarfs, as shown in **Figure 6** based on data from Lu et al. (2019) and Medina et al. (2020). Work by West et al. (2011) and Kiman et al. (2021) showed that the upward trend continues past the limits of **Figure 6** to the coolest M dwarfs, although when absolute *G* magnitudes are used instead of spectral types, the upward trend halts around $M_G \sim 15$ (corresponding to M7V) and drops for later types. It is worth noting that the samples are small and incomplete for the coolest M dwarfs, although additional observations continue to be added (Jeffers et al. 2018, Schöfer et al. 2019). Of course, increasing rates for cooler stars may be caused at least in part by the lower continuum fluxes at the wavelength of Hα that make relatively weak emission more easily detected.

Beyond canvassing for the presence or absence of an Hα emission line, additional work has been done to investigate Hα variability. Bell et al. (2012) surveyed 60 active M0–M8 dwarfs and found that M dwarfs with greater $L_{H\alpha}/L_{bol}$ were less variable, proposing that larger changes in magnetic activity levels are needed to produce measurable variability in Hα for the most active M dwarfs. For fully convective M dwarfs with masses of 0.1–0.3 $M_\odot$, Medina et al. (2020) found that stars with more frequent flares exhibit stronger Hα emission; they also found that 9 out of the 13 fully convective M dwarfs considered do not have Hα variability synchronized with rotation phase, so it is plausible that fixed spots or plages on the photosphere do not trigger Hα variability in the chromosphere.

Other spectral lines used to investigate M dwarf activity include the MgII h and k lines at 2795.5 Å and 2802.7 Å and the CaII H and K lines at 3933.7 Å and 3968.5 Å. These two doublets share similar formation characteristics and offer evidence of stellar chromospheres in M dwarfs (Cram & Mullan 1979). The lines have broadly damped wings and deep absorption cores that sometimes show central reemission because of magnetic activity. For comparison, the Sun's CaII K line manifests as an absorption line, which is indicative of the Sun's general magnetic inactivity. Despite the similarity of these two doublets, the CaII features form lower in the chromosphere than the Mg lines, as Ca atoms require lower ionization energies than Mg (Vernazza et al. 1981, Asplund et al. 2009). Walkowicz & Hawley (2009) discovered a linear correlation between the equivalent widths of Hα and CaII K for active mid-M dwarfs but noted that this correlation weakens for relatively inactive red dwarfs. Astudillo-Defru et al. (2017) investigated the strength of the CaII lines in M dwarfs using traditional S-index values, which they found to decrease with stellar mass from 0.60 to 0.35 $M_\odot$ and level off at lower masses. They suggested that this could be attributed to the transition of the stellar dynamo from partially to fully convective interiors.

M dwarf activity has also been explored spectroscopically using near- and far-UV bands, such as SiIII at 1206.5 Å, Lyα at 1215.67 Å, CII at 1335.71 Å, and HeII at 1640.4 Å. All of these lines have been found to be linearly related to the strengths of the Hα and CaII features in the optical band (Melbourne et al. 2020). When these high-energy photons impact the upper atmospheric

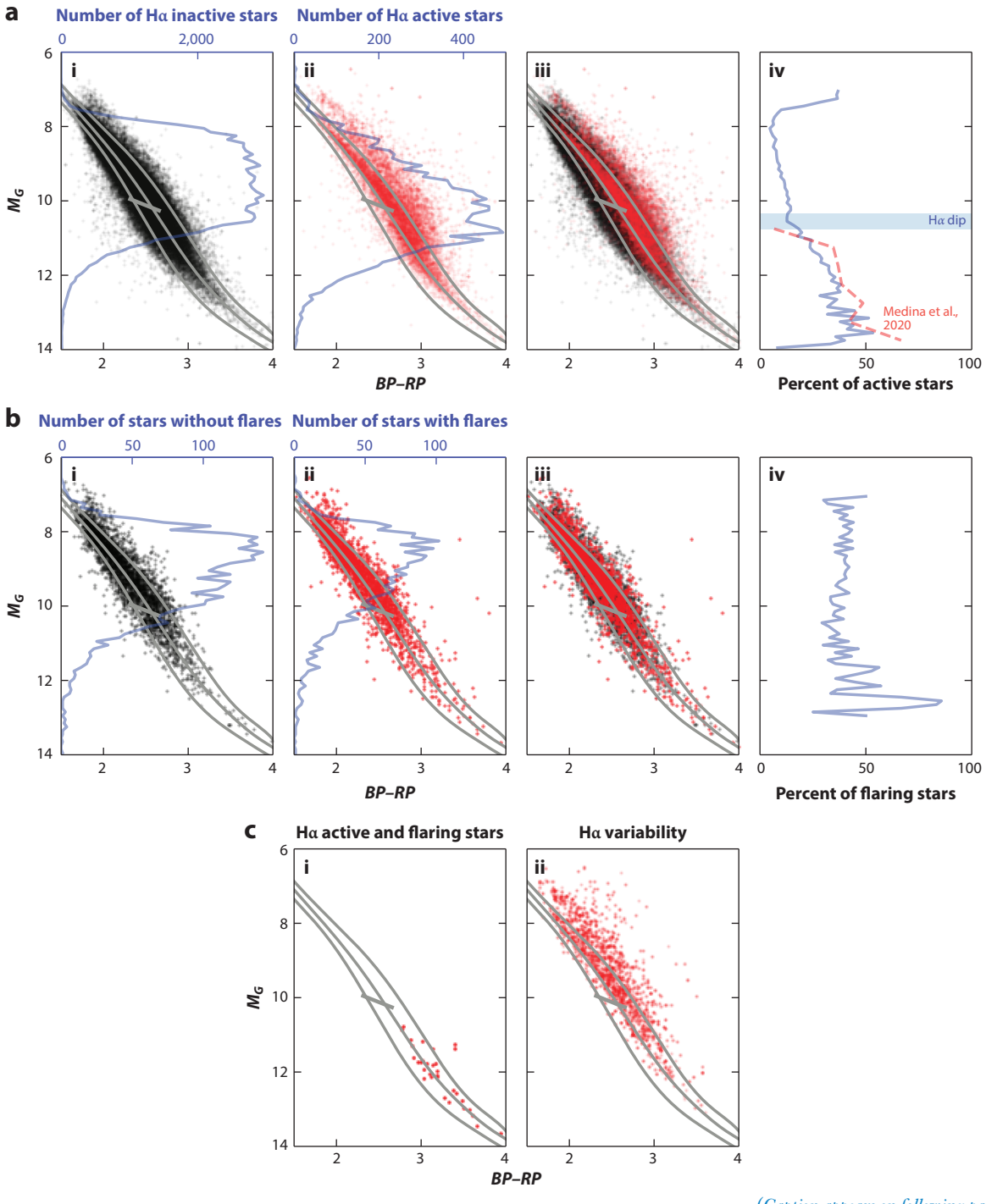

(*Caption appears on following page*)

Figure 6 (*Figure appears on preceding page*)

The distributions of various activity measurements are shown on Hertzsprung–Russell diagrams for M dwarfs of types M0V–M6V. Inactive and active stars have been extracted from Lu et al. (2019; Large Sky Area Multi-Object Fibre Spectroscopic Telescope) and Medina et al. (2020; MEarth). Gray lines represent the main sequence defined by Jao et al. (2023), and the gap between partially and fully convective stars is represented by the short angled line. (*a*) The distributions of Hα inactive (*i*, *black points*) and active (*ii*, *red points*) stars are shown, with the numbers of stars in each 0.1 M_G mag bin traced by blue lines in subpanels *i* and *ii* with scales given on the top. Subpanel *iii* overlaps the two distributions. Active M dwarfs are largely elevated above the fitted main sequence (Jao et al. 2023). Subpanel *iv* outlines the percentages of active stars in these plots with a solid blue line, and the dashed red line shows the consistent result from Medina et al. (2020). The blue-shaded region marks the Hα dip reported by Jao et al. (2023). (*b*) Stars without (*black points*) or with (*red points*) flares detected in *Kepler*, K2, and *Transiting Exoplanet Survey Satellite* data are plotted. Flare stars are found throughout the main sequence distribution, unlike that seen for Hα. The percentage of flaring M dwarfs in panel *iv* is relatively flat at around 40%. (*c*, *i*) Stars flagged as both Hα active and with flares by Medina et al. (2020). (*c*, *ii*) Stars with Hα variability per Lu et al. (2019).

gases of any orbiting exoplanets, they alter atmospheric chemistry, which is a consideration of some import when considering biospheres around M dwarfs.

6.2. Activity Detected Photometrically

There are three timescales of photometric variability relevant to M dwarfs: (*a*) short-term flare events that last minutes to hours, (*b*) medium-term changes due to the rotation of spots into and out of view that span hours to months, and (*c*) long-term variability caused by starspot cycles that are years to decades in duration. Here, we address each type of variability monitored photometrically at optical wavelengths.

6.2.1. Short-term flares. Flares are impulsive emissions resulting in flux increases for short periods of time that can be detected at optical wavelengths, particularly in the blue, because they have temperatures of 9,000–14,000 K in M dwarfs (Kowalski et al. 2013). An early effort to reveal flares on M dwarfs was the work of Bopp & Moffett (1973), who conducted 1-s high-cadence photoelectric, and simultaneous spectroscopic, observations over ∼30 min in the *U* filter of the close binary L 726-8 (BL and UV Ceti, M5.0Ve+M5.0Ve, 2.7 pc, with an orbital semimajor axis of 2.05 arcsec and period of 26 years; Benedict et al. 2016). Two fast-rise and exponential-decay flares were detected, and results revealed (*a*) an onset of Hβ and Hγ line emission occurring less than 2 min before the peak of the flare, (*b*) a 4-min delay to return to the quiescent line state after the flare, and (*c*) that these Balmer line profiles appeared to be asymmetric—a red asymmetry was detected before the flare maximum with excess emission in the red wings of the lines, followed by a blue excess after the flare maximum. Such line profile asymmetries are apparently caused by velocity gradients generated during the flare (Abbett & Hawley 1999).

In broader terms, Gershberg (1972) and Lacy et al. (1976) established the foundations for studying flare frequencies and energy levels among M dwarfs, revealing that lower-mass M dwarfs flare more often at lower energy levels than more massive M dwarfs. Hawley et al. (2014) adopted their protocol and carried out a detailed study of flare rates and energies for three inactive M dwarfs of types M1V–M3V and three active M dwarfs with Hα in emission of types M4V–M5V, all observed by the *Kepler* spacecraft at a 1-min cadence. They found that active stars exhibit numerous flares and clear rotational modulation due to starspots, whereas inactive stars have fewer flares and show weaker starspot signatures. They found no correlation of flare occurrence or energy with starspot phase. More recently, Günther et al. (2020) studied flares in 673 M dwarfs in TESS data, finding that white-light flares for M dwarfs have bolometric flare energies of 10^{31} to 10^{37} ergs, and confirmed past findings that fast rotating M dwarfs are the most likely to flare but that their flare amplitudes are independent of their rotation periods. Plots in **Figure 6*b*** show that ∼40% of M dwarfs with flares are distributed on either side of the median main sequence based on *Kepler* data (Lu et al. 2019), and that such a rate is relatively equal for all M dwarf types. Recent

research indicates that flares appear to occur at very high latitudes on red dwarfs (Ilin et al. 2021), so concerns about their effects on orbiting exoplanets may be less severe than first thought.

6.2.2. Medium-term rotation. Medium-term stellar variability is typically associated with the presence of starspots in the photosphere that cause brightness changes as a star rotates. The detectability of this variability, typically carried out using photometric techniques, hinges on the frequency and duration of observations. Recent missions like *Kepler*, *K2*, and TESS have proven to be ideal for the study of periodic signals ranging from fractions of a day to 20 days (McQuillan et al. 2013, Doyle et al. 2019). For rotational periods exceeding a month, ground-based endeavors like the Zwicky Transient Factory (ZTF) (Lu et al. 2019) and MEarth (Medina et al. 2020) allow magnetic activity and rotation studies of M dwarfs to be extended to several months.

Kraft (1967) carried out pioneering work making the connection between stellar rotation and CaII activity for solar-type stars. We now understand that this rotation-activity relation is closely related to stellar convection, differential rotation, magnetic field strength, and ages (Skumanich 1972, Stix 1976, Gilman 1980, Noyes et al. 1984). For example, in fast-rotating stars with convective zones at the surface, the stellar dynamos generate magnetic fields that emerge above the photosphere. These twisted magnetic fields drive the heating and cooling of the atmosphere, generating flares and/or starspots that can be monitored at various wavelengths. Skumanich (1972) first identified the rate of stellar spindown with age that is driven by magnetic braking, and this effect has been extended from FGK dwarfs to M dwarfs in clusters of various ages and in the Solar Neighborhood, as described by Wright et al. (2011). *Kepler*, *K2*, TESS, and the MEarth effort have enabled the identification of great numbers of stars with relatively low-level photometric changes, including work on younger stars (Rebull et al. 2016), fast rotating stars (Ramsay et al. 2020), and M dwarfs near the end of the main sequence (Pass & Charbonneau 2023).

Figure 7 provides an overview of M dwarf rotation for stars of various ages, using data from ZTF (Lu et al. 2022), *Kepler* (McQuillan et al. 2014), and *K2* (Reinhold & Hekker 2020, Popinchalk et al. 2021). Here, we assume the relative ages of the stars in the clusters are reliable, although the absolute ages remain somewhat uncertain. It is clear in **Figure 7*a*** that virtually all M dwarfs in clusters with ages of 120 Myr or less have rotation periods of a few hours to less than 10 days and that the overall spindown occurs from 10–750 Myr, and beyond. Note that some of the lowest-mass M dwarfs maintain their fast rotation, resulting in the oldest field star population bifurcating into clear fast- and slow-rotation sets of stars, with very few stars exhibiting intermediate rotation rates around 10 days. The six panels in **Figure 7*b*** show results for great numbers of M dwarfs, revealing three notable features in the M_G versus rotation period plane:

- There is an obvious gap in the distribution for partially radiative M dwarfs above the red bar that marks the partially/fully convective boundary. This characteristic has been extensively discussed since its discovery by McQuillan et al. (2014), with several different explanations summarized by Lu et al. (2022). The leading theory suggests that core-envelope coupling may be responsible for stalling the spindown in some stars (Spada & Lanzafame 2020), and that the radiative core conserves angular momentum, counteracting any potential spindown from magnetic braking.
- There is an underdensity region marked with red arrows, first identified by Lu et al. (2022) using ZTF results. It is possibly seen in *Kepler* data but is more difficult to discern in *K2* data, at least in part because of the relatively fast rotation cutoff for the dataset. Lu et al. (2022) proposed that these red dwarfs have poor faculae/spot contrast and low variability that is undetectable in ZTF data, yet this underdensity region may be seen in the higher-fidelity datasets. This region falls at the K/M dwarf transition zone at $M_G = 8.1$, a division that is empirically defined as the appearance of TiO bands in spectra. It seems unlikely that there

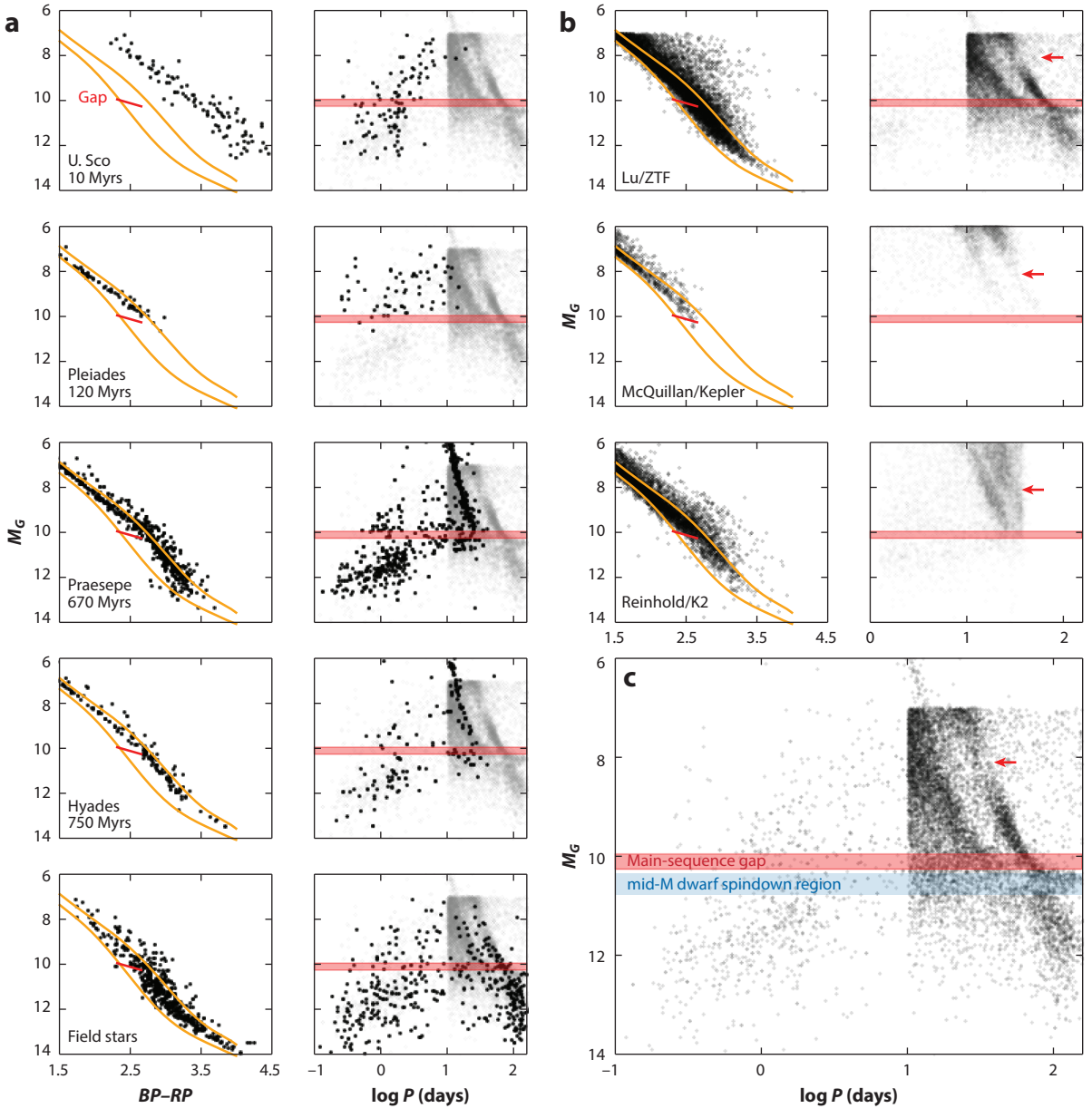

Figure 7

Rotation rates for M dwarfs with different ages are shown. (*a*) The Hertzsprung–Russell diagrams and M_G versus log rotation period distributions for five groups of M dwarfs with increasing ages from top to bottom. The upper and lower envelopes of the main sequence and the gap are plotted as orange and red lines, respectively, and a horizontal red band sketches the upper and lower limits of the main sequence gap. (*b*) Rotation rates from ZTF (Lu et al. 2022), *Kepler* (McQuillan et al. 2014), and *K2* (Reinhold & Hekker 2020) in the same format, although the period axes cover a more restricted range than in panel *a*. Red arrows mark the underdensity region discovered by Lu et al. (2022). (*c*) The sum of samples in the second column of panel *a* and the ZTF sample in the uppermost right subpanel of panel *b* is shown. The blue band shows the mid-M dwarf spindown region identified by Jao et al. (2023). Abbreviation: ZTF, Zwicky Transient Facility.

is a dip in spot coverage somehow connected to the spectroscopic division between late-K and early-M dwarfs, at least at relatively old ages, but any possible connection should be investigated.

- The third feature is a "spray" of slow rotators among M dwarfs just below the partially/fully convective gap, marked in **Figure 7*c*** with a blue band. Jao et al. (2023) first reported an Hα deficiency zone at $10.3 < M_G < 10.8$ and connected lower Hα activity to slower rotation rates in this region—the blue band in **Figure 7*c*** shows the same region as that shown in **Figure 6*a***, subpanel *iv*, linking the dip in Hα activity to the same stars with longer rotation periods. Jao et al. (2023) proposed that the spindown of these mid-M dwarfs may be linked to core-envelope decoupling. According to the ^{3}He instability model (Section 5.2), M dwarfs with masses of 0.30–0.32 $M_\odot$ could briefly form a radiative layer at ages of ∼40–250 Myr, followed by a fully convective stage. Some of these stars may spin down faster because the short-lived radiative layer affects the stars' angular momentum. In contrast, stars below 0.30 $M_\odot$ never create a radiative zone so their spindown follows the typical magnetic braking scenario.

In focused work on the lowest-mass, fully convective M dwarfs, Newton et al. (2017) found that stars with masses of ∼0.30 $M_\odot$ and rotation periods of less than 30 days are typically Hα active. This threshold increases to 80 days for 0.15 $M_\odot$ red dwarfs. In a related study, Pass & Charbonneau (2023) discovered that a substantial 74% of active, fully convective M dwarfs with masses of 0.1–0.3 $M_\odot$ are rapid rotators with periods less than 2 days. These rapid rotators may spin down to periods of 2–10 days over 1–3 Gyr and thereafter undergo a rapid spindown to periods of 80 days or longer as they age (Pass et al. 2022). For fully convective M dwarfs this causes the bimodal period distribution observed.

These results imply that as with other types of stars, for M dwarfs there are links among rotation, activity, and age. For example, Kiraga & Stepien (2007), Wright & Drake (2016), and Newton et al. (2017) all show a broken-law relation between rotation and activity for FGKM dwarfs, and the latter suggested that for K and M dwarfs the heating of the chromosphere that generates the Hα line may be independent from any underlying dynamo. Using great numbers of M dwarfs with both Hα and rotation measurements, Jao et al. (2023, their figure 14) showed that for partially radiative M dwarfs, fast rotators are generally elevated above the mean main sequence with a distribution that is shifted to redder, cooler stars at a given luminosity. For fully convective M dwarfs, the distributions of fast and slow rotators could not be distinguished on the HRD, suggesting that photospheric spot contrasts may be minimal, as previously discussed by Berdyugina (2005).

6.2.3. Long-term starspot cycles. A relatively new area of M dwarf research involves studies of long-term photometric variability in M dwarfs from years to decades; such studies are rare because of the need for extended commitment and resources. Weis (1994) pioneered the study of long-term M dwarf variability, examining 43 stars over 11 years using *VRI* photometry, finding that 21 exhibited detectable changes in brightness, with perhaps two that showed cycles lasting ∼3 years. Large-scale, long-term efforts that can now be used to study M dwarfs include the AAVSO (American Association of Variable Star Observers) Photometric All-Sky Survey (APASS), with ∼50-mmag precision at $V = 13$; the All-Sky Automated Survey (ASAS), with ∼100-mmag precision at $V = 13$; its more recent ASAS-SN extension with ∼15–25-mmag precision at $V = 13$–14; and the ZTF with ∼10–20-mmag precision at $r = 14$–17. Although none of these surveys specifically target M dwarfs, they do provide data that can be used to extract light curves for highly variable stars. For example, there are results from ASAS by Suárez Mascareño et al. (2016) reporting cycles for 31 M dwarfs with mean lengths around 7 years, and from

SMARTS: Small and Moderate Aperture Research Telescope System

ASAS/ASAS-SN (Irving et al. 2023) describing 12 cycles lasting 4–10 years. The *Gaia* mission and upcoming Vera C. Rubin Observatory effort will each produce datasets spanning roughly 10 years, offering great potential to detect many new stellar cycles with periods of a few years in M dwarfs, but periods longer than 10 years will remain new discovery territory.

There is one survey that already has more than 20 years of high-quality photometric data on M dwarfs. The RECONS effort at the CTIO/SMARTS (Small and Moderate Aperture Research Telescope System) 0.9-m telescope has been underway since 1999 and offers measurements at a precision of 5–10 mmag for M dwarfs with $VRI = 10$–16. **Figure 8** highlights four optical light curves from this program demonstrating long-term stellar activity in fully convective M stars

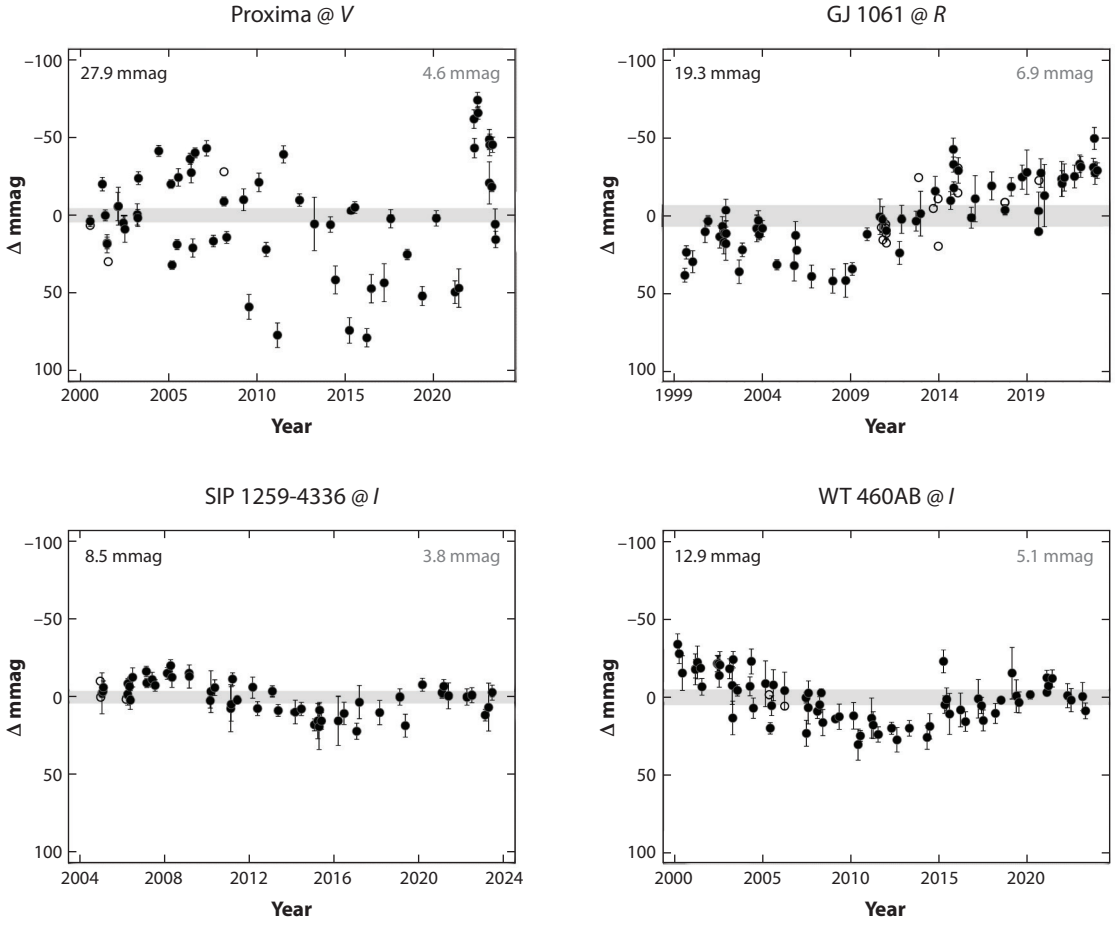

Figure 8

Four light curves for fully convective M dwarfs are shown, illustrating variability in the *VRI* bands over two decades of the REsearch Consortium On Nearby Stars program at the Cerro Tololo Inter-American Observatory/Small and Moderate Aperture Research Telescope System 0.9-m telescope. In these plots, a brightening star moves upward, where 10 mmag corresponds to an ∼1% change in flux. Typical 5-frame observational epochs taken during observing windows of ∼30 min are averaged and shown as black points, with error bars from the standard deviation of the frames; open circles indicate single-frame epochs. The MAD from the average of the shown data values is listed in black on the top left. Gray numbers in the top right of each panel are average MAD values for reference stars, also represented by the gray shaded regions above and below zero to show underlying noise levels. Figure provided by Andrew Couperus, who revised and updated the plots from Henry et al. (2018). Abbreviation: MAD, mean absolute deviation.

(updated from Henry et al. 2018 by Andrew Couperus). All four panels show stars' photometric measurements and variability values in the plots that are significantly greater than they are for the sets of comparison reference stars. The upper left panel shows 24 years of data at *V* for Proxima. Although large changes are evident owing to spots coming into and out of view over the 83-day rotation period (Benedict et al. 1998), there is no clear long-term spot cycle evident in the data. In contrast, the upper right panel illustrates the variability in the *R* band over 24 years for GJ 1061, a host of three reported exoplanets (Dreizler et al. 2020) with a rotation period of 180 days (Medina et al. 2020). This star demonstrates complex long-term activity spanning several decades with intermixed rotational variability. The two stars in the bottom panels exhibit clear starspot cycles evident in the *I* band, lasting ∼18 years for SIP 1259-4336 (M9.5Ve, 7.7 pc) and more than 20 years for WT 460AB (M5.0Ve, 9.1 pc; the B component is a low-mass stellar L dwarf companion that contributes minimal flux in the *I* band). Three of these stars showcase remarkable new observational territory, indicating that the smallest stars do, indeed, have spot cycles much like our Sun's. Future work will reveal M dwarfs with perhaps even longer cycles, including those of lower amplitude, as surveys with higher sensitivity become available. Already, curious results from theoretical work are evident, such as fully convective M dwarfs that appear to have magnetic fields strongly constrained to a single hemisphere (Brown et al. 2020). Such rich datasets will provide us with an understanding of the complex relations among rotation, stellar dynamos, and stellar cycles across the entire sequence of M dwarfs (Küker et al. 2019, Irving et al. 2023).

NUV band: spectral range of 1800–2750 Å

FUV band: spectral range of 1400–1700 Å

6.2.4. Photometric variability at X-ray and ultraviolet wavelengths. Stellar activity in red dwarfs can also be detected photometrically at wavelengths shorter than the optical. For example, Kowalski et al. (2010) detected a megaflare on YZ CMi (GJ 285, M4.0Ve, 6.0 pc) with an energy of 8.3×10^{30} ergs s^{-1} in the *U* band, which is equivalent to ∼37% the star's bolometric luminosity. Miles & Shkolnik (2017) reported that the level of variability in the NUV band increases with dropping temperatures for M dwarfs; such variability in the NUV is proposed to originate in the chromosphere (Stelzer et al. 2013). In contrast, no noticeable temperature trend is observed in the FUV band for M dwarfs using GALEX data (Miles & Shkolnik 2017). In the FUV band, active M dwarf flares are ∼10 times more energetic than those seen for inactive M dwarfs, but after normalizing for their quiescent fluxes, active and inactive M dwarfs exhibited the same flare distributions (Loyd et al. 2018). At higher energies, Mitra-Kraev et al. (2005) found that X-ray flares lag UV flares by an average of ten minutes and that the emission flux relationship between X-rays and UV appears to be linear (see also Stelzer et al. 2013). An important recent result by Magaudda et al. (2022) is that the X-ray luminosities of M dwarfs do not change significantly over time. By crossmatching X-ray detections for 687 K and M dwarfs in both *Rosat* and eROSITA data, they found that all but 65 change in luminosity by less than a factor of two, implying that X-ray levels are relatively steady for ∼90% of red dwarfs.

7. EXOPLANETS

Given their low masses and small radii, considerable effort has gone into revealing planets orbiting M dwarfs because highly coveted terrestrial worlds are more easily detected compared to searches around more massive G or K type stars—smaller planets cause larger signals when orbiting smaller stars using both radial velocity and transit methods. M dwarfs as hosts of exoplanets gained increased attention after the first planet was found orbiting the nearby star GJ 876 (Delfosse et al. 1998, Marcy et al. 1998). As the number of planets discovered around red dwarfs has swelled, there has been much debate about the habitability of worlds orbiting these stars because the stars themselves may have problematic characteristics. The debate hinges on key issues such as (*a*) tidal locking that forces one face of a planet to always be starward, thereby creating a hot side and a

cold side; (*b*) effects of variable flux levels at X-ray, UV, and optical wavelengths; and (*c*) the possible stripping of planetary atmospheres and oceans by stellar activity such as flares, which has been studied for more than two decades (Heath et al. 1999, Lingam & Loeb 2017; for a particular example, see Crossfield et al. 2022).

Jovian: a planet of mass $M > 0.41\,M_J$

Neptunian: a planet with mass in the range of $2\,M_\oplus < M < 0.41\,M_J$

Terrestrial: a planet of mass $M < 2\,M_\oplus$

Whether or not these issues preclude environments suitable for life remains currently unknown, and an analysis of these issues is beyond the scope of this review. Instead, we point the reader to an excellent overview by Tarter et al. (2007), who address potential issues related to biospheres on planets orbiting M dwarfs. That review is the result of an effort by several dozen scientists from various disciplines who attacked the problem head-on at an interdisciplinary workshop and reached the following circumspect conclusions:

> Tidally locked synchronous rotation within the narrow habitable zone does not necessarily lead to atmospheric collapse, and active stellar flaring may not be as much of an evolutionarily disadvantageous factor as has previously been supposed. We conclude that M dwarf stars may indeed be viable hosts for planets on which the origin and evolution of life can occur. (Tarter et al. 2007, p. 31)

Thus, M dwarfs remain compelling targets for the discovery of life-bearing worlds.

Here, we give a brief overview of planets reported to orbit M dwarfs, providing a snapshot of our current understanding as of September 2023, as gleaned from the NASA Exoplanet Archive.[4] Among the 280 red dwarfs within 10 pc, only 45 (16%) have been reported to have planets. More work remains to be done to pin down accurate population statistics, including searches for smaller planets, those in longer-period orbits, and those around active or faint red dwarfs where sensitivity challenges abound.

Reaching further to 100 pc in the NASA Exoplanet Archive provides a larger sample, albeit even more incomplete than the 10-pc sample and highly biased because of the heterogeneous way in which planet searches have been carried out. There are 187 M dwarfs closer than 100 pc with planets in the Archive as of September 2023. Of these, 87 are closer than 20 pc, and their planetary systems are shown schematically in **Figure 9**. The different types of exoplanets (jovian, neptunian, and terrestrial), detection methods, and the liquid water habitable zones for each system, estimated using the relation of Kopparapu et al. (2013), are illustrated. Considerations of orbital eccentricities are obfuscated here as some planets may dip in and out of the blue regions on the plot. Because different detection methods are implemented to detect exoplanets, their basic parameters, such as masses and radii, are not always available, and there is no doubt that low-mass planets and those in longer orbits have been missed. For example, planets detected only in radial velocity surveys have minimum mass values, and no radii are available. Transiting planets have measured radii and masses, but values require assumptions about the sizes and masses of the host stars, which usually must be estimated from relations. Nonetheless, terrestrial worlds falling in the habitable zones among these nearby M dwarfs include planets orbiting Ross 128, Wolf 1069, GJ 1061, GJ 1002, Proxima, Teegarden's Star, and TRAPPIST-1. Note that all of these stars are among the lowest-mass red dwarfs, a testament to the fact that small worlds are easier to detect around small stars.

The HRD in **Figure 9** outlines the M dwarfs with exoplanets closer than 20 pc, with the separation between partially and fully convective M dwarfs indicated. It is clear that both types of M dwarfs have planets, and we highlight a handful of systems here. AU Mic (GJ 803, M1.0, 9.7 pc) has a disk with potentially four (or more) planets (Plavchan et al. 2020, Donati et al. 2023) and is the primary in one of the two systems within 10 pc known to be younger than 100 Myr

[4]Many groups have published a great number of papers reporting exoplanets around M dwarfs. We refer the reader to the NASA Exoplanet Archive to retrieve any references desired.

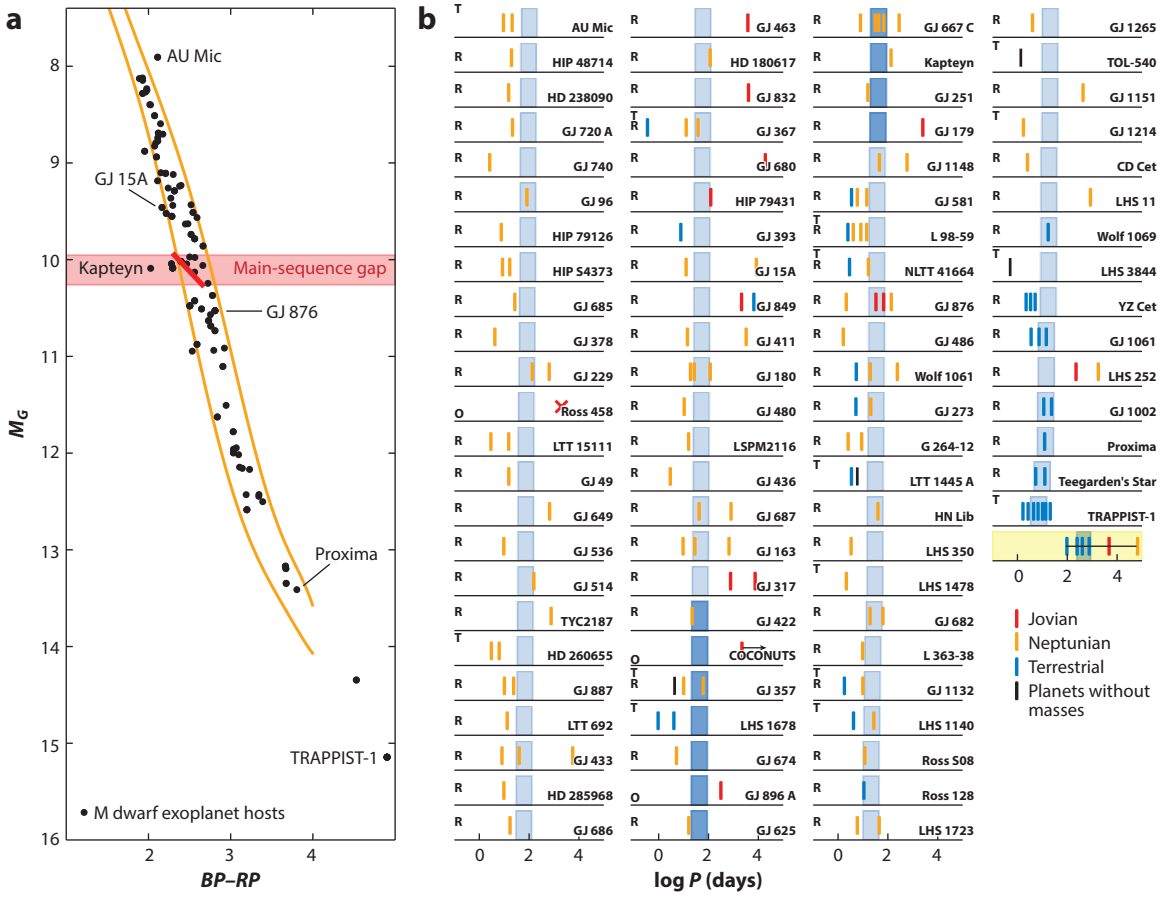

Figure 9

An overview of the 87 M dwarfs within 20 pc reported to have exoplanets from the NASA Exoplanet Archive as of September 2023. (*a*) An observational Hertzsprung–Russell diagram for the planet hosts. (*b*) Orbital periods for exoplanets in each system. The individual star panels are organized in decreasing M_G from top to bottom and left to right. Blue boxes in the panels indicate the estimated habitable zone for each star, wherein the inner edge is the limit for recent Venus and the outer edge is for early Mars. Habitable zones in darker blue are for stars in the pink shaded area in panel *a*, which marks the limits of the main sequence gap. Vertical bars indicate estimated or minimum masses listed in the Archive for jovian (*red*), neptunian (*orange*), and terrestrial (*blue*) planets as well as planets without masses (*black*). The discovery method for each system is labeled as "T," "R," or "O" for transiting, radial velocity, and other methods, respectively. The black arrow indicates a planet with an orbital period longer than 5 years, and the red X indicates that the orbital period is unknown. For comparison, the final panel with yellow shading shows our Solar System planets: Mercury, Venus, Earth, Mars, Jupiter, and Neptune.

(Section 4.1). GJ 15 A (M1.0V, 3.6 pc) has two reported planets (Howard et al. 2014, Pinamonti et al. 2018) and is in a wide binary with a second M dwarf, GJ 15 B (M3.5V), at a separation of 34 arcsec, corresponding to a projected distance of ~120 AU. GJ 876 (M3.5V, 4.7 pc) is the first M dwarf for which a planet was discovered (Delfosse et al. 1998, Marcy et al. 1998) and now has four reported planets (Rivera et al. 2010), including two jovians possibly in the habitable zone. Near the end of the main sequence are Proxima, which is now known to have at least one terrestrial planet (Anglada-Escudé et al. 2016) in its habitable zone, and TRAPPIST-1 (M7.5V, 12.5 pc), which harbors seven terrestrial worlds found via the transit method (Gillon et al. 2017). Overall, among planets reported around the 87 M dwarfs within 20 pc, most were found via radial

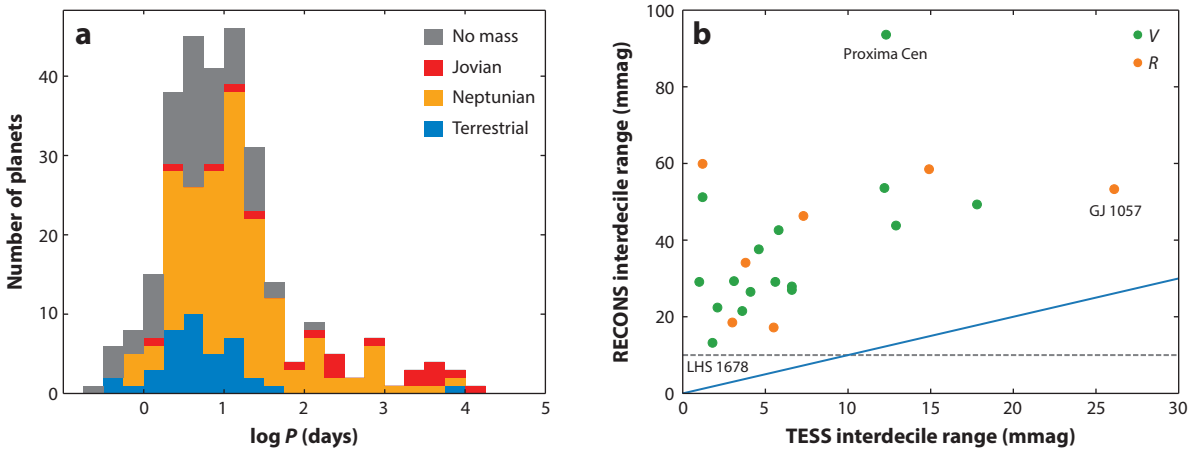

Figure 10

Two descriptions of planets orbiting M dwarfs are shown. (*a*) The stacked histogram shows the period distribution of reported exoplanets around M dwarfs within 100 pc, coded by color for the types of planets, as in **Figure 9**. Most detected planets have orbital periods less than 100 days; this is a consequence of limited time coverage in planet surveys. Note that most of the planets detected via radial velocity have only minimum mass estimates, so many characterizations of planets will shift to larger masses. Two additional jovian planets have orbital periods longer than 10^5 days and are not shown. All but one of the 74 planets without masses have measured radii—all but 2 are smaller than 4 $R_\oplus$. Overall, very few jovian planets are found orbiting M dwarfs. (*b*) A comparison between long-term variability over a decade or more from RECONS data in the *V* or *R* filters and medium-term variability over a month from TESS data in the spacecraft bandpass. The interdecile range for variability in millimagnitudes (mmag) is used for both timescales; for context, 1% = 10 mmag change in flux. Some stars are clearly less variable than others—Proxima and GJ 1057 are highly variable, and LHS 1678 is not. All stars change fluxes more over long timescales than short (equal changes would fall on the *solid blue line*), although some of the offset is expected because the TESS filter is redder than *V* or *R*. The gray dashed horizontal line indicates the effective detection limit in RECONS data; for TESS the limit is typically a few millimagnitudes for these stars, depending on source brightness. Panel *b* adapted from Kar et al. (2024) (CC BY 4.0) with permission from AAS. Abbreviations: RECONS, REsearch Consortium On Nearby Stars; TESS, *Transiting Exoplanet Survey Satellite*.

velocity work (so the masses are necessarily minimum estimates), and 15 systems have had at least one planet found during transit searches.

As shown in **Figure 9** for the nearest M dwarfs with planets and expanded to the full sample in **Figure 10*a***, most of the planets found around these small stars appear to be neptunian in mass. There is a substantial population of terrestrial worlds as well, and likely more yet to be discovered because they provide the weakest radial velocity and transit signals of all planets. Very few jovians, the most easily detected planets, have been found, and the few that have been reported are in relatively long orbits compared to lower-mass planets. A recent radial velocity survey of nearby, fully convective M dwarfs by Pass et al. (2023) has firmly confirmed this trend, finding that jovian planets around 0.1–0.3-$M_\odot$ stars are rare. There are planets reported to be orbiting both young stars (AU Mic and TOI-5205, the latter is at least elevated above the main sequence) and perhaps old stars (Kapteyn's Star, although the planet is suspect in this case; and Kepler-42, which may be relatively old). Although there are only a few M dwarfs in either age group reported to have planets, the implication is that planet formation is likely to have occurred throughout the history of the Milky Way, so large planet populations are inferred. Although the stellar multiplicity rate is 27% for M dwarfs (Section 4.2), only 13% (25 of 187) of the exoplanet hosts are known to have one or more stellar companions. These 25 systems all have wide stellar companions, and none of the exoplanets is in a circumbinary system, which appear to be quite rare, although caveats relating to target selection by exoplanet surveyors, e.g., avoiding binaries, are of course in play here.

Another consideration of habitability is often overlooked: What is the durability of the habitability? **Figure 10*b*** provides a first look at the variability of M dwarfs within 25 pc that host reported planets. Kar et al. (2024) have evaluated 23 stars with long-term photometric monitoring in the *V* or *R* filter over 10–23 years from the RECONS program as well as monthlong observations with TESS in the spacecraft bandpass is shown. Interdecile range measures are used to characterize these red dwarfs, corresponding to the range spanning 10–90% in fluxes. Proxima is the most variable over the long term (over 9%) and GJ 1057 is the most variable in TESS data, but still less than 3%. There is a group of stars that vary by less than 5% over a decade+ and less than 1% over a month that provides the most photometrically stable fluxes, at least at optical wavelengths. Overall variability is always greater over long timescales than over a month—all points lie above the one-to-one variability line shown in blue—although the TESS bandpass is redder than *V* or *R*, so the variability is inherently lower. To further understand the environments endured by planets orbiting M dwarfs, future efforts should focus on variability at higher energies than optical. Long-term monitoring at X-ray and UV wavelengths is currently difficult given constrained resources and the low fluxes provided by all but the most active M dwarfs, but the least variable stars are the ones likely to provide the most stable conditions for any potential biosphere.

8. DISCUSSION

Undoubtedly, red dwarfs play a leading role in the Solar Neighborhood and, by extension, in our Milky Way and in galaxies beyond. Below, we summarize various attributes of these ubiquitous stars, which can be highlighted with Three Laws of M Dwarfs:

1. M dwarfs account for three of every four stars.
2. M dwarf counts increase all the way to the end of the main sequence.
3. M dwarfs are partially radiative at high masses and fully convective at low masses.

Although not a single red dwarf can be seen with the naked eye from our planet, they are the most numerous denizens of our Galaxy. We have learned much about these small stars since their last review in this series nearly four decades ago, but future research areas are rich in possibilities. One example is the need for systematic searches that reveal the full suite of stellar, brown dwarf, jovian, neptunian, and terrestrial companions to red dwarfs. Even among the nearest ~3,000 red dwarf systems within 25 pc of the Sun, there are more companions of all types to be found, including presumably hundreds more solar systems. Ultimately, we predict that because of their numbers, proximity, and relative ease of investigation, the first truly Earth-like planet with life will be found orbiting a red dwarf.

SUMMARY POINTS

1. Red dwarfs dominate the stellar population, accounting for 75% of all stars.
2. Red dwarfs vary in mass more than any other type of hydrogen-burning star, by a factor of eight. A similar range in mass stretches from ~5.0 $M_\odot$ to 0.61 $M_\odot$, which spans spectral types mid-B through K. Their numbers increase all the way to the end of the main sequence, and even though each one of them is relatively low in mass compared to other stars, they are in fact the primary contributors to the stellar mass in the Solar Neighborhood.
3. Red dwarf primaries have stellar companions roughly one-quarter of the time, whereas the secondaries are stars more than ten times as often as they are brown dwarfs. Stellar

companions are in circular orbits if the periods are less than about a week but rarely are in circular orbits at periods of 5–30 years.

4. Red dwarfs are the only type of main sequence star that presents a gap in their distribution on the main sequence. This is due to a separation of partially radiative to fully convective stars near 0.35 $M_{\odot}$.
5. Red dwarfs exhibit photometric and spectroscopic variability on short, medium, and long timescales. These stars show a clear bifurcation of rotation periods, with few stars spinning once in ∼10 days and many rotating at faster and slower rates. They also exhibit spot cycles that last from a few years to more than two decades.
6. Red dwarfs have been reported to be orbited by planets of all sizes, with jovian types rarely found, whereas neptunian and terrestrial worlds are common.

DISCLOSURE STATEMENT

The authors are not aware of any affiliations, memberships, funding, or financial holdings that might be perceived as affecting the objectivity of this review.

ACKNOWLEDGMENTS

We especially thank several young scientists in the RECONS group who have provided results discussed here before publication: Andrew Couperus, Aman Kar, Madison LeBlanc, and Eliot Vrijmoet. We also thank many additional past students who have assisted with various facets of the RECONS effort over the past 25 years, including Tom Beaulieu, Mark Boyd, Misty Brown, Tiffany Clements, Serge Dieterich, Charlie Finch, Altonio Hosey, John Lurie, Leonardo Paredes, Adric Riedel, Justin Rodriguez, R. Andrew Sevrinsky, Michele Silverstein, John Subasavage, and Jennifer Winters. More senior collaborators over the years who contributed invaluable advice and effort include Fabien Baron, G. Fritz Benedict, Edgardo Costa, Greg Feiden, Otto Franz, David Golimowski, Nigel Hambly, Elliott Horch, Phil Ianna, David Koerner, Rene Mendez, Ed Nelan, Doug Simons, Ken Slatten, and Andrei Tokovinin, and the authors are indebted to each of them.

LITERATURE CITED

Abbett WP, Hawley SL. 1999. *Ap. J.* 521(2):906–19
Adams WS, Joy AH, Humason ML. 1926. *Ap. J.* 64:225–42
Adams WS, Kohlschutter A. 1914. *Ap. J.* 39:341–49
Aerts C. 2021. *Rev. Mod. Phys.* 93:015001
Allard F. 2014. In *Exploring the Formation and Evolution of Planetary Systems, IAU Symp. 299*, ed. M Booth, BC Matthews, JR Graham, pp. 271–72. Cambridge, UK: Cambridge Univ. Press
Allred JC, Kowalski AF, Carlsson M. 2015. *Ap. J.* 809:104
Alonso-Floriano FJ, Morales JC, Caballero JA, et al. 2015. *Astron. Astrophys.* 577:A128
Anglada-Escudé G, Amado PJ, Barnes J, et al. 2016. *Nature* 536:437–40
Asplund M, Grevesse N, Sauval AJ, Scott P. 2009. *Annu. Rev. Astron. Astrophys.* 47:481–522
Astudillo-Defru N, Delfosse X, Bonfils X, et al. 2017. *Astron. Astrophys.* 600:A13
Baraffe I, Chabrier G. 2018. *Astron. Astrophys.* 619:A177
Baraffe I, Chabrier G, Allard F, Hauschildt PH. 1997. *Astron. Astrophys.* 327:1054–69
Baraffe I, Chabrier G, Allard F, Hauschildt PH. 1998. *Astron. Astrophys.* 337:403–12
Barnard EE. 1916. *Astron. J.* 29:181–83

Baroch D, Morales JC, Ribas I, et al. 2018. *Astron. Astrophys.* 619:A32
Basri G. 2021. *An Introduction to Stellar Magnetic Activity*. Bristol, UK: IOP Publ.
Bell KJ, Hilton EJ, Davenport JRA, et al. 2012. *Publ. Astron. Soc. Pac.* 124(911):14–20
Benedict GF, Henry TJ, Franz OG, et al. 2016. *Astron. J.* 152(5):141
Benedict GF, McArthur B, Nelan E, et al. 1998. *Astron. J.* 116:429–39
Benz AO, Güdel M. 2010. *Annu. Rev. Astron. Astrophys.* 48:241–87
Berdyugina SV. 2005. *Liv. Rev. Solar Phys.* 2:8
Berger DH, Gies DR, McAlister HA, et al. 2006. *Ap. J.* 644:475–83
Bergfors C, Brandner W, Janson M, et al. 2010. *Astron. Astrophys.* 520:A54
Bessell MS. 1982. *Proc. Astron. Soc. Aust.* 4:417–19
Best WMJ, Dupuy TJ, Liu MC, Siverd RJ, Zhang Z. 2020. The UltracoolSheet: Photometry, Astrometry, Spectroscopy, and Multiplicity for 3000+ Ultracool Dwarfs and Imaged Exoplanets. The UltracoolSheet Catalog, updated Nov. 1, retrieved March 2023. **http://bit.ly/UltracoolSheet**
Bochanski JJ, Hawley SL, Covey KR, et al. 2010. *Astron. J.* 139(6):2679–99
Bochanski JJ, West AA, Hawley SL, Covey KR. 2007. *Astron. J.* 133:531–44
Boeshaar PC. 1976. *The spectral classification of M-dwarf stars*. PhD Thesis, Ohio State Univ., Columbus
Bonfils X, Delfosse X, Udry S, et al. 2005. *Astron. Astrophys.* 442:635–42
Bopp BW, Moffett TJ. 1973. *Ap. J.* 185:239–52
Boudreaux TM, Chaboyer BC. 2023. *Ap. J.* 944(2):129
Boyajian TS, von Braun K, van Belle G, et al. 2012. *Ap. J.* 757:112
Brown BP, Oishi JS, Vasil GM, Lecoanet D, Burns KJ. 2020. *Ap. J. Lett.* 902:L3
Burgasser AJ, Kirkpatrick JD, Burrows A, et al. 2003. *Ap. J.* 592:1186–92
Cannon AJ, Pickering EC. 1918. *Ann. Harv. Coll. Obs.* 91:1–290
Cantrell JR, Henry TJ, White RJ. 2013. *Astron. J.* 146(4):99
Castelli F, Kurucz RL. 2003. Poster presented at *Modelling of Stellar Atmospheres*, IAU Symp. 210, poster A20
Chabrier G, Baraffe I, Phillips M, Debras F. 2023. *Astron. Astrophys.* 671:A119
Chabrier G, Küker M. 2006. *Astron. Astrophys.* 446(3):1027–37
Charbonneau P. 2014. *Annu. Rev. Astron. Astrophys.* 52:251–90
Cortés-Contreras M, Béjar VJS, Caballero JA, et al. 2017. *Astron. Astrophys.* 597:A47
Covey KR, Ivezić Ž, Schlegel D, et al. 2007. *Astron. J.* 134(6):2398–417
Cram LE, Mullan DJ. 1979. *Ap. J.* 234:579–87
Crossfield IJM, Malik M, Hill ML, et al. 2022. *Ap. J. Lett.* 937:L17
Dahn CC, Harris HC, Levine SE, et al. 2008. *Ap. J.* 686:548–59
Dantona F, Mazzitelli I. 1986. *Astron. Astrophys.* 162(1–2):80–86
Davenport JRA. 2016. *Ap. J.* 829:23
Delfosse X, Forveille T, Beuzit JL, et al. 1999. *Astron. Astrophys.* 344:897–910
Delfosse X, Forveille T, Mayor M, et al. 1998. *Astron. Astrophys.* 338:L67–70
Delfosse X, Forveille T, Ségransan D, et al. 2000. *Astron. Astrophys.* 364:217–24
Demory BO, Ségransan D, Forveille T, et al. 2009. *Astron. Astrophys.* 505:205–15
Dieterich SB, Henry TJ, Golimowski DA, Krist JE, Tanner AM. 2012. *Astron. J.* 144(2):64
Dieterich SB, Henry TJ, Jao WC, et al. 2014. *Astron. J.* 147:94
Donati JF, Cristofari PI, Finociety B, et al. 2023. *MNRAS* 525:455–75
Donati JF, Morin J, Petit P, et al. 2008. *MNRAS* 390(2):545–60
Dorman B, Nelson LA, Chau WY. 1989. *Ap. J.* 342:1003–18
Doyle L, Ramsay G, Doyle JG, Wu K. 2019. *MNRAS* 489:437–45
Dreizler S, Jeffers SV, Rodríguez E, et al. 2020. *MNRAS* 493:536–50
Dupuy TJ, Liu MC. 2017. *Ap. J. Suppl. Ser.* 231:15
Eggen OJ, Greenstein JL. 1967. *Ap. J.* 150:927–42
Feiden GA. 2016. *Astron. Astrophys.* 593:A99
Feiden GA, Chaboyer B. 2012. *Ap. J.* 757:42
Feiden GA, Chaboyer B. 2014. *Ap. J.* 789:53
Feiden GA, Skidmore K, Jao WC. 2021. *Ap. J.* 907:53

Fischer DA, Valenti J. 2005. *Ap. J.* 622:1102–17
Gaia Collab., Brown AGA, Vallenari A, et al. 2018. *Astron. Astrophys.* 616:A1
Gaia Collab., Smart RL, Sarro LM, et al. 2021. *Astron. Astrophys.* 649:A6
Gaia Collab., Vallenari A, Brown AGA, et al. 2023. *Astron. Astrophys.* 674:A1
Gershberg RE. 1972. *Ap. Space Sci.* 19:75–92
Giclas HL, Burnham R, Thomas NG. 1971. *Lowell proper motion survey Northern Hemisphere. The G numbered stars. 8991 stars fainter than magnitude 8 with motions >0.″26/year*. Flagstaff, AZ: Lowell Obs.
Gill S, Maxted PFL, Evans JA, et al. 2019. *Astron. Astrophys.* 626:A119
Gillon M, Triaud AHMJ, Demory BO, et al. 2017. *Nature* 542(7642):456–60
Gilman PA. 1980. In *IAU Colloq. 51: Stellar Turbulence*, Vol. 114, ed. DF Gray, JL Linsky, pp. 19–37. Berlin: Springer-Verlag
Gizis JE. 1997. *Astron. J.* 113:806–22
Gizis JE, Reid IN. 2000. *Publ. Astron. Soc. Pac.* 112:610–13
González-Payo J, Cortés-Contreras M, Lodieu N, et al. 2021. *Astron. Astrophys.* 650:A190
Gould BA. 1881. *Astron. Nachr.* 100:7
Gray RO, Corbally CJ, Garrison RF, et al. 2006. *Astron. J.* 132:161–70
Günther MN, Zhan Z, Seager S, et al. 2020. *Astron. J.* 159(2):60
Gustafsson B, Edvardsson B, Eriksson K, et al. 2008. *Astron. Astrophys.* 486(3):951–70
Hauschildt PH, Allard F, Baron E. 1999. *Ap. J.* 512:377–85
Hawley SL, Davenport JRA, Kowalski AF, et al. 2014. *Ap. J.* 797(2):121
Hawley SL, Gizis JE, Reid IN. 1996. *Astron. J.* 112:2799–827
Heath MJ, Doyle LR, Joshi MM, Haberle RM. 1999. *Orig. Life Evol. Biosph.* 29(4):405–24
Heber U. 2009. *Annu. Rev. Astron. Astrophys.* 47:211–51
Hejazi N, Lépine S, Nordlander T. 2022. *Ap. J.* 927:122
Henry TJ. 1991. *A systematic search for low mass companions orbiting nearby stars and the calibration of the end of the stellar main sequence*. PhD Thesis, University of Arizona
Henry TJ, Franz OG, Wasserman LH, et al. 1999. *Ap. J.* 512:864–73
Henry TJ, Ianna PA, Kirkpatrick JD, Jahreiss H. 1997. *Astron. J.* 114:388–95
Henry TJ, Jao WC, Subasavage JP, et al. 2006. *Astron. J.* 132(6):2360–71
Henry TJ, Jao WC, Winters JG, et al. 2018. *Astron. J.* 155(6):265
Henry TJ, Kirkpatrick JD, Simons DA. 1994. *Astron. J.* 108:1437–44
Henry TJ, McCarthy DW Jr. 1990. *Ap. J.* 350:334–47
Henry TJ, McCarthy DW Jr. 1993. *Astron. J.* 106:773–89
Henry TJ, Walkowicz LM, Barto TC, Golimowski DA. 2002. *Astron. J.* 123(4):2002–9
Horch EP, van Altena WF, Demarque P, et al. 2015. *Astron. J.* 149:151
Howard AW, Marcy GW, Fischer DA, et al. 2014. *Ap. J.* 794:51
Ianna PA, Bessell MS. 1986. *Publ. Astron. Soc. Pac.* 98:658–61
Ilin E, Poppenhaeger K, Schmidt SJ, et al. 2021. *MNRAS* 507(2):1723–45
Irving ZA, Saar SH, Wargelin BJ, do Nascimento JD. 2023. *Ap. J.* 949(2):51
Irwin J, Buchhave L, Berta ZK, et al. 2010. *Ap. J.* 718(2):1353–66
Irwin JM, Quinn SN, Berta ZK, et al. 2011. *Ap. J.* 742(2):123
Janson M, Bergfors C, Brandner W, et al. 2014. *Ap. J.* 789(2):102
Janson M, Hormuth F, Bergfors C, et al. 2012. *Ap. J.* 754:44
Jao WC, Feiden GA. 2021. *Res. Notes Am. Astron. Soc.* 5(5):124
Jao WC, Henry TJ, Beaulieu TD, Subasavage JP. 2008. *Astron. J.* 136:840–80
Jao WC, Henry TJ, Gies DR, Hambly NC. 2018. *Ap. J. Lett.* 861:L11
Jao WC, Henry TJ, Subasavage JP, et al. 2011. *Astron. J.* 141:117
Jao WC, Henry TJ, White RJ, et al. 2023. *Astron. J.* 166(2):63
Jao WC, Mason BD, Hartkopf WI, Henry TJ, Ramos SN. 2009. *Astron. J.* 137:3800–8
Jao WC, Nelan EP, Henry TJ, Franz OG, Wasserman LH. 2016. *Astron. J.* 152:153
Jeffers SV, Schöfer P, Lamert A, et al. 2018. *Astron. Astrophys.* 614:A76
Johnson HL, Morgan WW. 1953. *Ap. J.* 117:313–52

Joy AH. 1947. *Ap. J.* 105:96–104
Joy AH, Humason ML. 1949. *Publ. Astron. Soc. Pac.* 61(360):133–34
Kar A, Henry TJ, Couperus AA, Vrijmoet EH, Jao W-C. 2024. *Astron. J.* 167(5):196
Kesseli AY, Kirkpatrick JD, Fajardo-Acosta SB, et al. 2019. *Astron. J.* 157(2):63
Kiman R, Faherty JK, Cruz KL, et al. 2021. *Astron. J.* 161(6):277
Kippenhahn R, Schlüter A. 1957. *Zeitschr. Astrophys.* 43:36
Kiraga M, Stepien K. 2007. *Acta Astron.* 57:149–72
Kirkpatrick JD, Henry TJ, McCarthy DW. 1991. *Ap. J. Suppl. Ser.* 77:417–40
Kirkpatrick JD, Reid IN, Liebert J, et al. 1999. *Ap. J.* 519(2):802–33
Kopparapu RK, Ramirez R, Kasting JF, et al. 2013. *Ap. J.* 765(2):131
Kowalski AF, Hawley SL, Holtzman JA, Wisniewski JP, Hilton EJ. 2010. *Ap. J. Lett.* 714:L98–102
Kowalski AF, Hawley SL, Wisniewski JP, et al. 2013. *Ap. J. Suppl. Ser.* 207:15
Kraft RP. 1967. *Ap. J.* 150:551–70
Kuiper GP. 1939. *Ap. J.* 89:548–51
Kuiper GP. 1940. *Ap. J.* 91:269–72
Kuiper GP. 1942. *Ap. J.* 95:201–12
Kukarkin BV, Parenago PP. 1958. *Obshchiĭ katalog peremennykh zvezd. Soderzhashchee svedenii'a o 14 708 peremennykh zvezdakh, otkrytykh i oboznachennykh do 1958 goda*. Moskva: Izd-vo Akad. nauk SSSR
Küker M, Rüdiger G, Olah K, Strassmeier KG. 2019. *Astron. Astrophys.* 622:A40
Lachaume R, Rabus M, Jordán A, et al. 2019. *MNRAS* 484(2):2656–73
Lacy CH, Moffett TJ, Evans DS. 1976. *Ap. J. Suppl. Ser.* 30:85–96
Lane BF, Boden AF, Kulkarni SR. 2001. *Ap. J. Lett.* 551:L81–83
Lawson PR, ed. 2000. *Principles of long baseline stellar interferometry*. JPL Publ. 00-009 07/00. **https://core.ac.uk/download/pdf/79046071.pdf**
Lépine S, Rich RM, Shara MM. 2003. *Ap. J. Lett.* 591:L49–52
Lépine S, Rich RM, Shara MM. 2007a. *Ap. J.* 669:1235–47
Lépine S, Rich RM, Shara MM, Cruz KL, Skemer A. 2007b. *Ap. J.* 668:507–12
Liebert J, Probst RG. 1987. *Annu. Rev. Astron. Astrophys.* 25:473–519
Limber DN. 1958. *Ap. J.* 127:387–427
Lindgren S, Heiter U. 2017. *Astron. Astrophys.* 604:A97
Lingam M, Loeb A. 2017. *Ap. J.* 848:41
Linsky JL, Bornmann PL, Carpenter KG, et al. 1982. *Ap. J.* 260:670–94
López-Morales M. 2007. *Ap. J.* 660:732–39
López-Morales M, Ribas I. 2005. *Ap. J.* 631:1120–33
Loyd ROP, France K, Youngblood A, et al. 2018. *Ap. J.* 867:71
Lu Hp, Zhang Ly, Shi J, et al. 2019. *Ap. J. Suppl. Ser.* 243(2):28
Lu YL, Curtis JL, Angus R, David TJ, Hattori S. 2022. *Astron. J.* 164(6):251
Luyten WJ. 1926. *Harv. Coll. Obs. Bull.* 835:2–3
Luyten WJ. 1938. *MNRAS* 98:677–79
Luyten WJ. 1949. *Ap. J.* 109:532–36
Luyten WJ. 1968. *MNRAS* 139:221–24
Luyten WJ. 1979. *New Luyten catalogue of stars with proper motions larger than two tenths of an arcsecond (NLTT)*. Minneapolis, MN, updated June 2019. **https://heasarc.gsfc.nasa.gov/W3Browse/star-catalog/nltt.html**
Lynn WT. 1872. *MNRAS* 33:102–3
MacDonald J, Gizis J. 2018. *MNRAS* 480:1711–14
Magaudda E, Stelzer B, Raetz S, et al. 2022. *Astron. Astrophys.* 661:A29
Mann AW, Deacon NR, Gaidos E, et al. 2014. *Astron. J.* 147(6):160
Mann AW, Dupuy T, Kraus AL, et al. 2019. *Ap. J.* 871:63
Mansfield S, Kroupa P. 2021. *Astron. Astrophys.* 650:A184
Marcy GW, Butler RP, Vogt SS, Fischer D, Lissauer JJ. 1998. *Ap. J. Lett.* 505(2):L147–49
Marfil E, Tabernero HM, Montes D, et al. 2021. *Astron. Astrophys.* 656:A162

Martin DV, Sethi R, Armitage T, et al. 2023. *MNRAS* 528:963–75
McQuillan A, Aigrain S, Mazeh T. 2013. *MNRAS* 432(2):1203–16
McQuillan A, Mazeh T, Aigrain S. 2014. *Ap. J. Suppl. Ser.* 211(2):24
Medan I, Lépine S. 2023. *MNRAS* 521:208–29
Medina AA, Winters JG, Irwin JM, Charbonneau D. 2020. *Ap. J.* 905(2):107
Melbourne K, Youngblood A, France K, et al. 2020. *Astron. J.* 160(6):269
Michelson AA, Pease FG. 1921. *Ap. J.* 53:249–59
Miles BE, Shkolnik EL. 2017. *Astron. J.* 154(2):67
Mitra-Kraev U, Harra LK, Güdel M, et al. 2005. *Astron. Astrophys.* 431:679–86
Montes D, González-Peinado R, Tabernero HM, et al. 2018. *MNRAS* 479:1332–82
Morales JC, Ribas I, Jordi C, et al. 2009. *Ap. J.* 691(2):1400–11
Morgan WW. 1938. *Ap. J.* 87:589–91
Morgan WW, Keenan PC, Kellman E. 1943. *An Atlas of Stellar Spectra, with an Outline of Spectral Classification*. Chicago: Univ. Chic. Press
Mould JR. 1976a. *Astron. Astrophys.* 48(3):443–59
Mould JR. 1976b. *Ap. J.* 210:402–15
Newton ER, Irwin J, Charbonneau D, et al. 2017. *Ap. J.* 834:85
Newton ER, Mann AW, Tofflemire BM, et al. 2019. *Ap. J. Lett.* 880:L17
Noyes RW, Hartmann LW, Baliunas SL, Duncan DK, Vaughan AH. 1984. *Ap. J.* 279:763–77
Osterbrock DE. 1953. *Ap. J.* 118:529–46
Parsons SG, Gänsicke BT, Marsh TR, et al. 2018. *MNRAS* 481:1083–96
Pass EK, Charbonneau D. 2023. *Ap. J.* 949(2):37
Pass EK, Charbonneau D, Irwin JM, Winters JG. 2022. *Ap. J.* 936(2):109
Pass EK, Winters JG, Charbonneau D, et al. 2023. *Astron. J.* 166:11
Passegger VM, Bello-García A, Ordieres-Meré J, et al. 2022. *Astron. Astrophys.* 658:A194
Pecaut MJ, Mamajek EE. 2013. *Ap. J. Suppl. Ser.* 208:9
Pickles AJ. 1998. *Publ. Astron. Soc. Pac.* 110(749):863–78
Pinamonti M, Damasso M, Marzari F, et al. 2018. *Astron. Astrophys.* 617:A104
Plavchan P, Barclay T, Gagné J, et al. 2020. *Nature* 582(7813):497–500
Popinchalk M, Faherty JK, Kiman R, et al. 2021. *Ap. J.* 916(2):77
Popper DM. 1980. *Annu. Rev. Astron. Astrophys.* 18:115–64
Ramsay G, Doyle JG, Doyle L. 2020. *MNRAS* 497(2):2320–26
Rebull LM, Stauffer JR, Bouvier J, et al. 2016. *Astron. J.* 152(5):113
Reid IN. 1987. *MNRAS* 225:873–901
Reid IN, Hawley SL. 2005. *New Light on Dark Stars: Red Dwarfs, Low-Mass Stars, Brown Dwarfs*. Berlin/Heidelberg: Springer
Reid IN, Hawley SL, Gizis JE. 1995. *Astron. J.* 110:1838–59
Reiners A, Basri G. 2006. *Astron. J.* 131:1806–15
Reiners A, Basri G. 2009. *Astron. Astrophys.* 496(3):787–90
Reiners A, Zechmeister M, Caballero JA, et al. 2018. *Astron. Astrophys.* 612:A49
Reinhold T, Hekker S. 2020. *Astron. Astrophys.* 635:A43
Reylé C, Jardine K, Fouqué P, et al. 2021. *Astron. Astrophys.* 650:A201
Riaz B, Gizis JE, Samaddar D. 2008. *Ap. J.* 672:1153–58
Riedel AR, Finch CT, Henry TJ, et al. 2014. *Astron. J.* 147:85
Riedel AR, Murphy SJ, Henry TJ, et al. 2011. *Astron. J.* 142(4):104
Riedel AR, Subasavage JP, Finch CT, et al. 2010. *Astron. J.* 140(3):897–911
Rivera EJ, Laughlin G, Butler RP, et al. 2010. *Ap. J.* 719:890–99
Rojas-Ayala B, Covey KR, Muirhead PS, Lloyd JP. 2012. *Ap. J.* 748(2):93
Roman NG. 1955. *Ap. J. Suppl. Ser.* 2:195–223
Ross FE. 1926. *Astron. J.* 36:124–28
Scalo JM. 1986. *Fundam. Cosmic Phys.* 11:1–278
Schöfer P, Jeffers SV, Reiners A, et al. 2019. *Astron. Astrophys.* 623:A44

Ségransan D, Kervella P, Forveille T, Queloz D. 2003. *Astron. Astrophys.* 397:L5–8
Serenelli A, Weiss A, Aerts C, et al. 2021. *Astron. Astrophys. Rev.* 29:4
Silverstein ML. 2019. *Sizing up red dwarfs in the solar neighborhood*. PhD Thesis, Ga. State Univ., Atlanta
Skrutskie MF, Forrest WJ, Shure M. 1989. *Astron. J.* 98:1409–17
Skumanich A. 1972. *Ap. J.* 171:565–68
Sneden CA. 1973. *Carbon and nitrogen abundances in metal-poor stars*. PhD Thesis, Univ. Texas, Austin
Somers G, Cao L, Pinsonneault MH. 2020. *Ap. J.* 891:29
Souto D, Cunha K, Smith VV, et al. 2020. *Ap. J.* 890(2):133
Spada F, Lanzafame AC. 2020. *Astron. Astrophys.* 636:A76
Stauffer JR, Hartmann LW. 1986. *Ap. J. Suppl. Ser.* 61:531–68
Stelzer B, Marino A, Micela G, López-Santiago J, Liefke C. 2013. *MNRAS* 431(3):2063–79
Stix M. 1976. *Astron. Astrophys.* 47(2):243–54
Stromgren B. 1952. *Astron. J.* 57:65–83
Suárez Mascareño A, Rebolo R, González Hernández JI. 2016. *Astron. Astrophys.* 595:A12
Tarter JC, Backus PR, Mancinelli RL, et al. 2007. *Astrobiology* 7:30–65
Torres G, Andersen J, Giménez A. 2010. *Astron. Astrophys. Rev.* 18:67–126
Torres G, Ribas I. 2002. *Ap. J.* 567(2):1140–65
Udry S, Mayor M, Delfosse X, Forveille T, Perrier-Bellet C. 2000. In *Birth and Evolution of Binary Stars*, *Poster Proceedings of IAU Symp. 200*, ed. B Reipurth, H Zinnecker, pp. 158–60. Cambridge, UK: Cambridge Univ. Press
Valenti JA, Piskunov N. 1996. *Astron. Astrophys. Suppl. Ser.* 118:595–603
van Altena WF, Lee JT, Hoffleit ED. 2001. *VizieR Online Data Catalog*, I/238A. **https://vizier.cds.unistra.fr/viz-bin/VizieR-3?-source=I/238A/picat&-out.max=50&-out.form=HTML%20Table&-out.add=_r&-out.add=_RAJ,_DEJ&-sort=_r&-oc.form=sexa**
van Maanen A. 1940. *Ap. J.* 91:503–5
van Saders JL, Pinsonneault MH. 2012. *Ap. J.* 751:98
Vernazza JE, Avrett EH, Loeser R. 1981. *Ap. J. Suppl. Ser.* 45:635–725
Vrijmoet EH. 2023. *Orbital architectures of M dwarf companions*. PhD Thesis, Ga. State Univ., Atlanta
Vrijmoet EH, Henry TJ, Jao WC, Dieterich SB. 2020. *Astron. J.* 160(5):215
Vrijmoet EH, Tokovinin A, Henry TJ, et al. 2022. *Astron. J.* 163(4):178
Walkowicz LM, Hawley SL. 2009. *Astron. J.* 137(2):3297–313
Wanderley F, Cunha K, Souto D, et al. 2023. *Ap. J.* 951(2):90
Ward-Duong K, Patience J, De Rosa RJ, et al. 2015. *MNRAS* 449(3):2618–37
Weis EW. 1994. *Astron. J.* 107:1135–40
West AA, Hawley SL, Bochanski JJ, et al. 2008. *Astron. J.* 135(3):785–95
West AA, Morgan DP, Bochanski JJ, et al. 2011. *Astron. J.* 141(3):97
Wing RF, Dean CA, MacConnell DJ. 1976. *Ap. J.* 205:186–93
Winters JG, Henry TJ, Jao WC, et al. 2019. *Astron. J.* 157(6):216
Winters JG, Irwin JM, Charbonneau D, et al. 2020. *Astron. J.* 159(6):290
Wolf M. 1919. *Veroeffentlichungen Badischen Sternwarte Heidelberg* 10:195–219
Woolf VM, Lépine S, Wallerstein G. 2009. *Publ. Astron. Soc. Pac.* 121(876):117–24
Woolf VM, Wallerstein G. 2004. *MNRAS* 350(2):575–79
Woolf VM, Wallerstein G. 2005. *MNRAS* 356(3):963–68
Wright NJ, Drake JJ. 2016. *Nature* 535(7613):526–28
Wright NJ, Drake JJ, Mamajek EE, Henry GW. 2011. *Ap. J.* 743:48
Youngblood A, France K, Loyd ROP, et al. 2017. *Ap. J.* 843:31
Zhang Ly, Meng G, Long L, et al. 2021. *Ap. J. Suppl. Ser.* 253:19
Zhang S, Luo AL, Comte G, et al. 2019. *Ap. J. Suppl. Ser.* 240(2):31
Zhang ZH, Galvez-Ortiz MC, Pinfield DJ, et al. 2018. *MNRAS* 480(4):5447–74
Ziegler C, Law NM, Baranec C, Riddle RL, Fuchs JT. 2015. *Ap. J.* 804:30